学位論文（要約）

Study of proton single-particle states in oxygen isotopes via the (p,2p) reaction at 250 MeV/u

（核子あたり250 MeVでの(p,2p)反応による
酸素同位体の陽子一粒子状態の研究）

平成28年3月博士（理学）申請

東京大学大学院理学系研究科物理学専攻
川瀬 頌一郎

Study of proton single-particle states in oxygen isotopes via the $(p, 2p)$ reaction at 250 MeV/u

Doctoral Dissertation
by

Kawase Shoichiro

March, 2016

Department of Physics, Graduate School of Science,
University of Tokyo
Hongo 7-3-1, Bunkyo-ku, Tokyo 113-0033, Japan

Abstract

A study was conducted to clarify the dependence of the reduction of single particle strength on separation energy differences and to determine the proton 0p spin-orbit splitting in oxygen isotopes.

For this purpose, we have measured the cross sections for the $(p, 2p)$ reaction on ^{14,22,24}O at 250 MeV/u at the RI Beam Factory at RIKEN. The solid polarized proton target was used in the measurement of the $(p, 2p)$ reaction in inverse kinematics for the first time.

The strengths of the single-hole states in nitrogen isotopes were successfully extracted. The measured cross section was compared to the DWIA calculations with the global Dirac phenomenology optical potential and the microscopic optical model. Spectroscopic factors for the transitions from oxygen isotopes to nitrogen isotopes for the $(p, 2p)$ reaction were determined for the first time.

The reduction ratio R_s of the spectroscopic factor has no significant dependence on the proton/neutron separation energy difference ΔS that was observed in the analysis of measurements of nucleon knockout reaction by using heavy-ion injections. The independence of R_s from S_N implies the universality of the tensor effect affecting the single particle strength in the nuclei.

The spin-orbit splitting of 0p proton orbits in ^{14}O was also determined to be 7.6±0.3 MeV. This value is larger than that of ^{16}O by 600 keV and consistent with the spin-orbit splitting for 0p neutrons evaluated from the ^{14}C(p, d) reaction measurement. However, it is opposite to the decrease expected from the description that the spin-orbit splitting is affected from the strong attractive interaction between the spin-flip isospin-flip partner.

Contents

List of Figures

List of Tables

Chapter 1

Introduction

1.1 Single-particle nature in atomic nuclei

The atomic nucleus, which is located at the core of an atom, is a quantum mechanical system which consists of only two kinds of fermions: protons and neutrons. Because there are only two basic components of nuclei, all the isotopes can be identified by the numbers of protons and neutrons. The difference of the proton number (Z) determines the number of bound electrons in a neutral atom and therefore results in the difference of the chemical property of the atom. The number of neutron (N) is limited by the possible range of the mass-to-charge ratio ($A/Z = 1 + N/Z$). In spite of only two kinds and limited number of ingredients, nuclei appear in astonishing variety of forms.

In 1935, Weizsäcker [1] proposed a famous mass formula with an assumption of *liquid drop* model and it successfully explained the mass of nuclei. This model is based on the characteristics of the nuclear force that is so strong and works in short-range. Such characteristics are consistent with Yukawa's meson theory [2]. The liquid-drop model succeeded also in the description of the mechanism of the nuclear fission [3].

Meanwhile, in early 1930's, Elsasser [4] had pointed out that the nucleus is particularly stable when it has a *magic number*, or the specific number of protons or neutrons. Currently known magic numbers are 2, 8, 20, 28, 50, 82, and 126. The existence of these magic numbers implies the picture that nucleons are moving independently in the mean-field as an analogy to the atomic structure. However, this picture apparently conflicts with the strong-interacting picture.

In late 1940's, these empirical magic numbers are successfully reproduced independently by Mayer and Jensen [5, 6], by introducing a simple modification to the harmonic oscillator potential. They added an attractive term $\propto l^2$ and a strong spin-orbit term $-\vec{l}\cdot\vec{s}$ with the opposite sign to that of atoms. This success confirmed the effectivity of independent particle model (IPM). What is very surprising is that strong-interacting particles behave rather independently in atomic nuclei! The characteristics of the ground state such as energy and spin are well explained by IPM in which non-interacting nucleons are orbiting in spherical symmetric mean-field potential.

However, IPM could not explain the nature of excited states or open-shell nuclei. To understand them, the idea of the shell-model configuration mixing was introduced [7, 8] and established a great success. The configuration mixing is invoked by the residual interactions which were not included in the mean-field potential. On the configuration-mixing basis, the shell-model single-particle orbit in nuclear mean-field potential is not fully occupied even if the single-particle energy is below the Fermi energy. Long-range correlations couple valence

nucleons to surface phonons and giant resonances. On the other hand, short range correlations which mainly originated from the nucleon hardcore, or the strong short-range repulsive NN force, couples the strength of valence nucleons to high-momentum component. The excitation probability to the high energy (momentum) state caused by such correlations results in the overestimation of low-lying single-particle strengths in mean field calculations since the high-energy states are greatly truncated in those calculations.

For the qualitative discussion of the single-particle strength, a quantity named spectroscopic factor has been traditionally used because the occupation number of single-particle orbit is not an observable. The definition of the spectroscopic factor is twofold. One is the experimental spectroscopic factor which is defined as the ratio between the reaction cross section measured in the experiment and the one calculated for unit occupation number of a single particle orbit in some reaction theory:

$$C^2S_{\mathrm{exp}} = \frac{\sigma_{\mathrm{exp}}}{\sigma^{\mathrm{sp}}_{\mathrm{theory}}}. \tag{1.1}$$

The other is theoretical spectroscopic factor which is defined as the squared overlap of the multi-particle wave function of A nuclei and that of the system of $A-1$ nuclei plus a nucleon in a specific single-particle orbit with certain quantum numbers:

$$C^2S_{\mathrm{theory}} = \left|\left\langle N_{nlj} \otimes (A-1) \,\middle|\, A \right\rangle\right|^2. \tag{1.2}$$

This value is generally calculated by using some mean-field models.

As mentioned previously, it is known that the spectroscopic factor observed in the experiment suffer a reduction from the theoretical predictions based on the mean-field calculations [9]. Figure 1.1 [10] shows the summed spectroscopic strength observed for proton knockout by the $(e, e'p)$ reaction from various single-particle orbits in the closed-shell nuclei as a function of the mean excitation energy of each single-particle orbit relative to the Fermi energy; weakly-bound states are on the right. Here the spectroscopic strength is defined as the ratio of the spectroscopic factor obtained in the experiment to the one resulted from the mean-field calculation. The solid line shows the fully microscopic theoretical calculation for nuclear matter and the dashed curve shows the one including surface effects for ^{208}Pb [11].

In this figure, the spectroscopic strength would be 1 if the mean-field theory were the complete description. However, the actual data show the 30–40% reduction of the proton spectroscopic strength from the theoretical calculation. Such reduction is attributed to the residual interaction in mean-field model, namely short-range and tensor correlations, which decrease the single-particle strength below the Fermi energy and populate the states above it [10]. The binding energy dependence of the reduction ratio is consistent with the intuitive understanding: the weaker binding reduces the occupation number.

Recently, Gade and Tostevin reported that the reduction ratio has strong correlation with the difference of separation energies between protons and neutrons [12, 13] by using nucleon-knockout reactions with heavy-ion injection. Figure 1.2 shows the correlation of the reduction ratio R_s and the difference in separation energies of the proton and the neutron $\Delta S = S_p - S_n$. R_s is defined as follows:

$$R_s \equiv \frac{\sigma_{\mathrm{exp}}}{\sigma_{\mathrm{th}}} = \frac{C^2S_{\mathrm{exp}}}{C^2S_{\mathrm{theory}}}, \tag{1.3}$$

There is a strong negative correlation between R_s and ΔS. The authors claimed that it is due to the increase of the correlation in the nucleus and accordingly the single-particle nature is suppressed. However, this suggests that more deeply bound nucleons has stronger correlations.

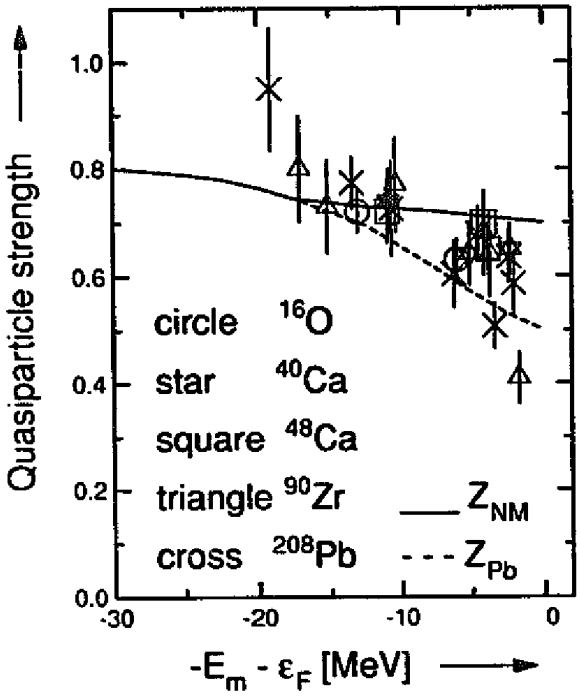

Figure 1.1: Total spectroscopic strength observed for proton knockout as a function to the excitation energy (quoted from Ref. [10]). E_m is the mean excitation energy for each orbit and ϵ_F is the Fermi energy. The solid and the dashed lines show the strengths calculated for nuclear matter with a realistic nucleon-nucleon interactions without and with surface effects, respectively.

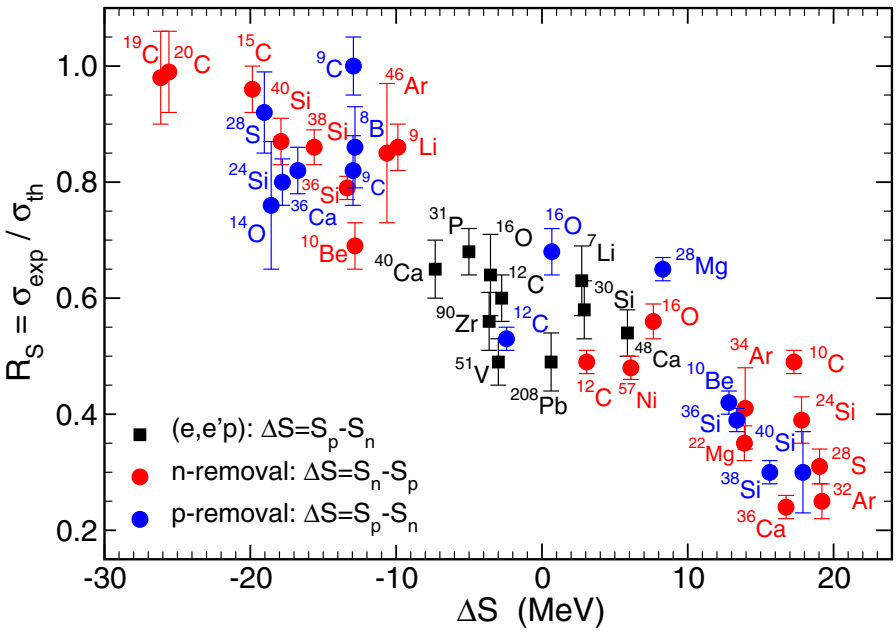

Figure 1.2: Reduction of the measured nucleon knockout cross sections relative to theoretical values as a function of the difference in separation energies of the two nucleon species, ΔS (quoted from Ref. [13]).

It is quite unnatural. This picture directly contradicts to an intuitive model that the weaker binding reduces the occupation number.

Several studies were carried out to investigate the reduction factor by using other reactions. Consequently, the dependence is not observed in the (p, d) neutron transfer reaction at the energy of 33 MeV/u [14] and in the (d, t) and $(d,^3\mathrm{He})$ reactions at the energy of 18.1 MeV/u [15]. Figure 1.3 shows the R_s for argon isotopes obtained by using both of transfer reactions (red circles) and knockout reaction with heavy-ion injections (blue triangles). There is clear discrepancy of R_s between n-transfer and n-knockout measurements. Figure 1.4 shows the R_s for oxygen isotopes obtained by using $(d,^3\mathrm{He})$ and (d, t) reactions. For this time, the reason of the difference of the correlation is not well understood. Therefore more information is needed to understand the problem by using other reaction probes.

For this purpose, the $(p, 2p)$ reaction would be the best probe because of its simple reaction mechanism and reliable theoretical descriptions. In this work, the author determined R_s for the ground states of ^{14}O ($\Delta S = -18.552$ MeV) and ^{24}O ($\Delta S = 22.92$ MeV) with the $(p, 2p)$ reaction. ^{14}O and ^{24}O comes in the far left and the right region of R_s in Figs. 1.2, 1.3, and 1.4. Since the reaction is well described by theoretical model, the presented data will be a large help for understanding the reduction mechanism of the single-particle strength.

1.2 Spin-orbit splitting in nuclei

In association with the single particle nature of nuclei, the magic number is one of the hottest topics in nuclear physics. The magic number had been considered to be constant through the study on stable nuclei for a long period since Mayer and Jensen's time. The development of the experimental method using radioactive isotope (RI) beams brings the nuclear physics toward new horizons [16]. It enables experiments with unstable nuclei and many dramatic phenomena which cannot be predicted from the study of stable nuclei were discovered. One of those is the disappearance of conventional magic numbers [17, 18] and the appearance of new magic numbers [19, 20] in unstable nuclei. The change of spin-orbit coupling, which was introduced to explain the origin of magic numbers, is cited as one of major factors.

The spin-orbit coupling arises mainly from three microscopic origins [21, 22]. Two body LS force accounts for approximately half of the coupling. The remaining half is shared by the two-body tensor force which dominated by one-pion exchange [23, 24, 25], and three-body forces [26] by two-pion exchange.

Usually the spin-orbit potential is approximated to be proportional to the first derivative of the central potential:

$$V_{\mathrm{so}}(r) \propto -\frac{1}{r}\frac{d}{dr}U_{\mathrm{cent}}(r)\,\vec{l}\cdot\vec{s}. \tag{1.4}$$

In unstable nuclei, the binding is weaker than the stable nuclei and as a result, the strength of the spin-orbit coupling becomes smaller. Several theoretical calculations predicted that the energy splitting between spin-orbit partners becomes smaller in drip-line nuclei because of the weakening of spin-orbit coupling [27].

The spin-orbit coupling cannot be directly measured through experiments but the spin-orbit splitting, which results from the spin-orbit coupling, is a experimentally measurable value and directly linked to the strength of the spin-orbit coupling. The spin-orbit coupling is defined as the energy difference between the spin-orbit partner, or the spin-doublet, in independent particle model. As illustrated in Fig. 1.5, the single-particle orbits in extreme of the independent particle model are generally fragmented into a bunch of shell model states through the configuration mixing due to the residual interaction. All the states which are observed in the experiment

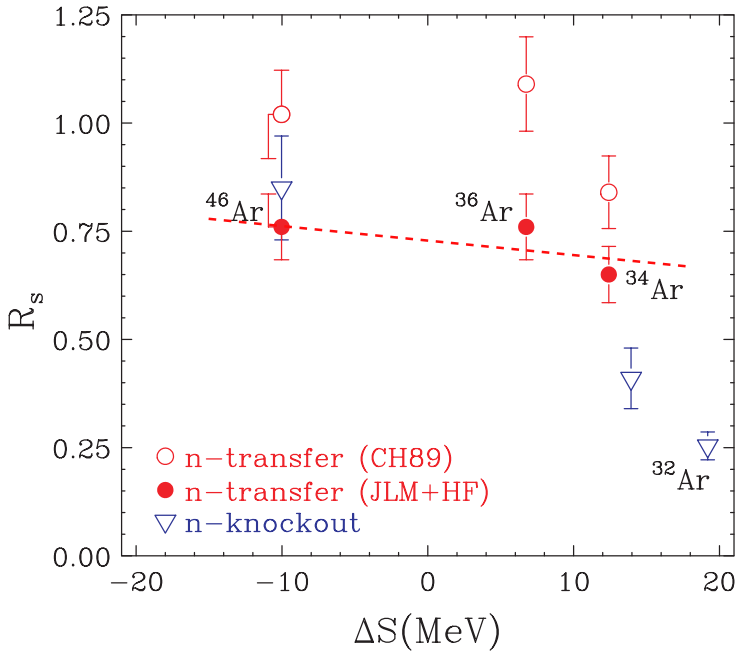

Figure 1.3: Reduction factors R_s for argon isotopes as a function of the difference between neutron and proton separation energies, ΔS (quoted from Ref. [14]). With the transfer reaction (red circles), No significant dependence on ΔS which was observed in the knockout reaction measurement with heavy ions (blue triangles) was not seen. The red dashed line is an eye guide drawn by the author.

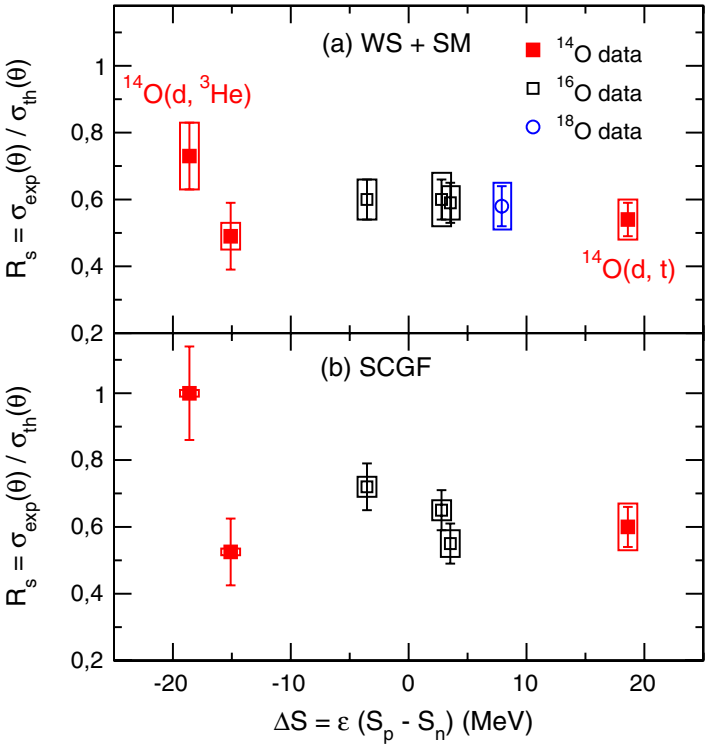

Figure 1.4: Reduction factors R_s for oxygen isotopes as a function of the difference between neutron and proton separation energies, ΔS (quoted from Ref. [15]).

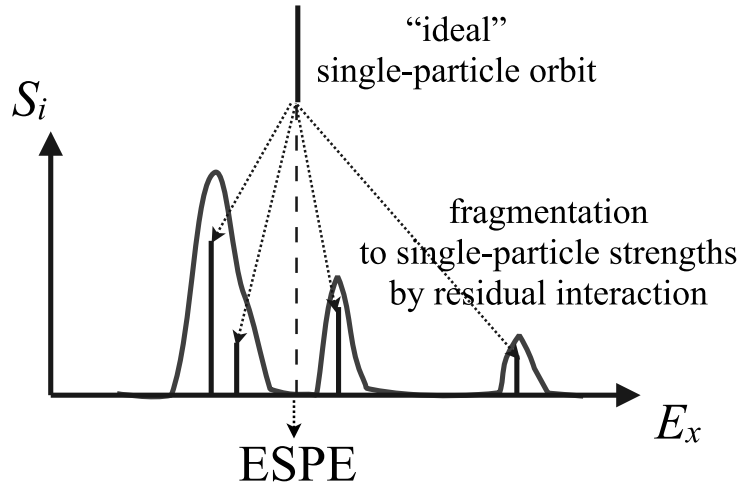

Figure 1.5: Fragmentation of single-particle orbit and effective single particle energy.

are after the fragmentation, therefore the energy of the "original" single-particle state have to be estimated in some fashion. For that purpose, the effective single particle energy (ESPE) is introduced. One of the definition of ESPE is the spectroscopic-factor-weighted mean of excitation energies of the states having certain J^π:

$$\mathrm{ESPE} = \frac{\sum E_x C^2 S_i}{\sum C^2 S_i}. \tag{1.5}$$

Here, E_x is the excitation energy for each state and C^2S_i is the spectroscopic factor which signifies how strong the single particle nature remains in the states of atomic nuclei as mentioned in the previous section.

In this study, the spin-orbit splitting is defined as follows:

$$\Delta E_{\mathrm{so}} = \mathrm{ESPE}_{j<} - \mathrm{ESPE}_{j>}. \tag{1.6}$$

$j_<$ and $j_>$ stand for the states of spin-doublet with $J = L - 1/2$ and $L + 1/2$.

The author has carried out the experiment for the determination of 0p spin-orbit splitting, *i.e.* the ESPE difference between $0p_{1/2}$ and $0p_{3/2}$ orbits, in oxygen stable isotopes ^{16}O and ^{18}O [28] by using the exclusive measurement of the $(p, 2p)$ reaction in normal kinematics. The spin-orbit splitting in ^{18}O is reduced compared to that of ^{16}O both in $(p, 2p)$ and $(d,^3\mathrm{He})$ experiments. The difference of $(p, 2p)$ and $(d,^3\mathrm{He})$ is due to the reduction of the excitation energy acceptance of $(d,^3\mathrm{He})$ above $\sim$ 10 MeV due to the momentum matching. There is a large change of the spin-orbit splitting even in stable isotopes, therefore more dramatic changes are expected in unstable isotopes. The determination of the spin-orbit splitting in unstable isotopes is one of the goals in this study.

1.3 Reaction probes for single-particle/hole states

For the study of single-particle/hole states of nuclei, selectivity to the single-particle/hole states is required for the reaction probes. In addition, the sensitivity to the total angular momentum J is also needed. In this section, the reactions which are used for the study of single-particle orbits are briefly explained.

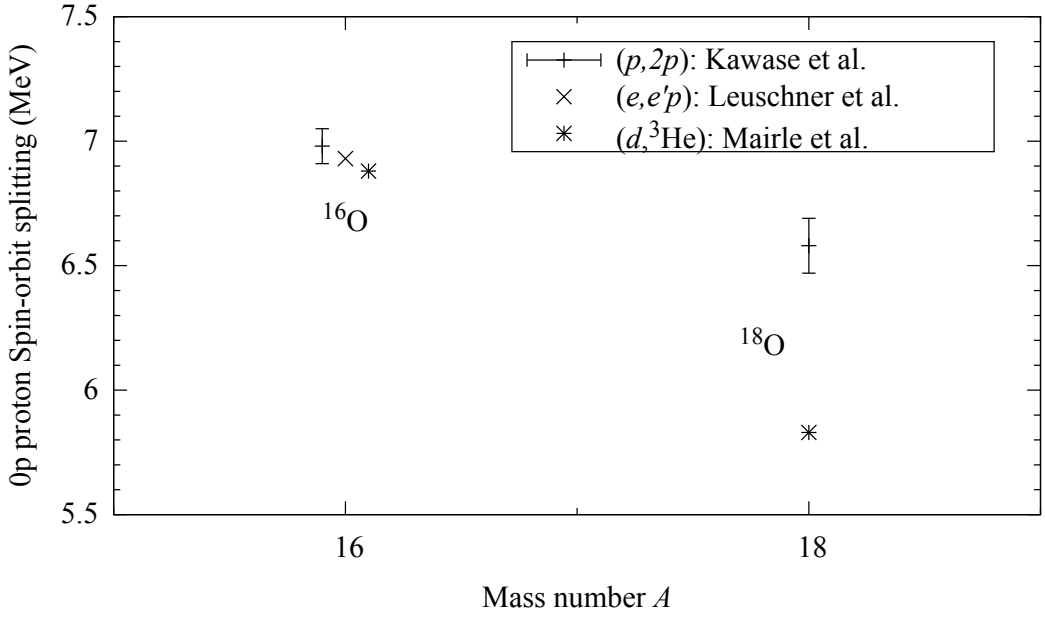

Figure 1.6: 0p spin-orbit splitting in oxygen stable isotopes [28]

Nucleon transfer reactions

The nucleon transfer reaction includes not only pickup reactions but also stripping reactions. Pickup reactions such as (p,d), (t,α) or $(d,^3\mathrm{He})$ are applied to investigate single-particle states. while stripping reactions such as (d,p), $(^3\mathrm{He},\alpha)$, or $(^3\mathrm{He},t)$ are for single-hole states. For the analysis, usually Distorted-Wave Born Approximation (DWBA) method is used for the discussion of cross sections and angular distributions [29, 30]. The angular distribution of the cross section is used to the determination of the orbital angular momentum l. For single-nucleon orbits, J can also be deduced from the (vector) analyzing power A_y. A_y is a quantity which indicates the spin-asymmetry of the reaction and expressed as[1]

$$A_y(\theta) = \frac{C}{P}\left(\frac{\sigma_\uparrow(\theta) - \sigma_\downarrow(\theta)}{\sigma_\uparrow(\theta) + \sigma_\downarrow(\theta)}\right) \tag{1.7}$$

where $\sigma_\uparrow(\theta)$ and $\sigma_\downarrow(\theta)$ are the cross sections of the reaction with the spin-polarized beam, P is the polarization of the beam, and a constant factor C is 1 for spin 1/2 and 3/2 for spin 1 particles.

Figure 1.7 shows the angular distributions of the vector analyzing powers for the transitions with $p_{1/2}$ and $p_{3/2}$ orbits for the $^{40}\mathrm{Ca}(d,p)^{41}\mathrm{Ca}$ reaction [31]. In this figure, the vector analyzing powers have opposite signs for $p_{1/2}$ and $p_{3/2}$ states and thus one can determine J for the states whose J is not determined.

The nucleon transfer reactions have large cross sections at intermediate energy region $<$ 100 MeV/u because of the momentum matching condition [32]. Due to the its moderate energy, the reaction becomes more sensitive to the surface region than the $(p,2p)$ reaction which favors higher energy region.

The study of transfer reaction on unstable isotopes in inverse kinematics has some difficulty due to its kinematics conditions. In spite of the low intensity of radioactive beams, the lower energy of the recoil particle requires thinner reaction target and the resulting reaction yields suffer from the thin target.

[1]Tensor polarization for spin 1 particle is ignored here.

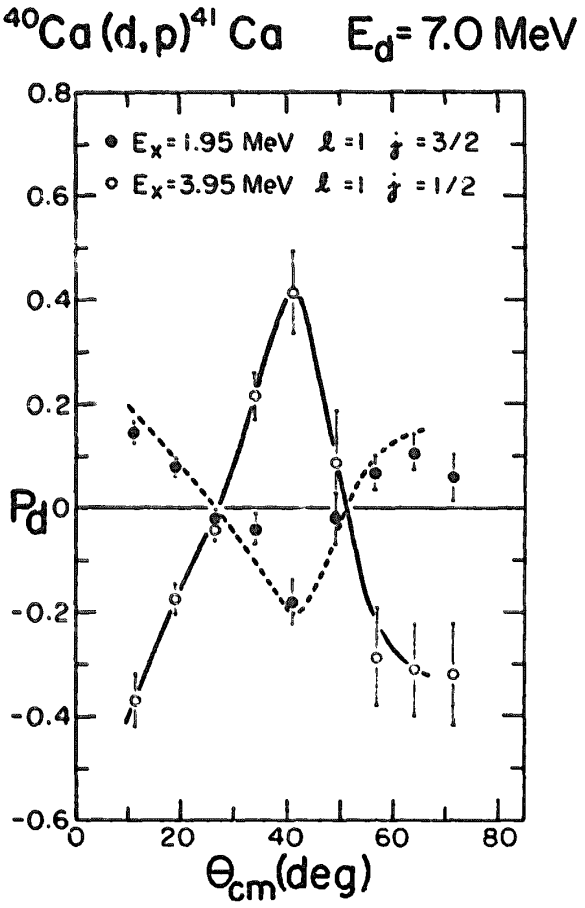

Figure 1.7: The angular distributions of the vector analyzing powers for the ^{40}Ca$(d,p)^{41}$Ca reaction (quoted from Ref. [31]). The definition of P_d is identical to A_y for spin 1 particle in the text.

Quasi-free electron-proton scattering

The quasi-free electron-proton scattering $(e,e'p)$ was also used to investigate the single-particle structure of nuclei. Since electrons have little interaction with neutrons, this reaction is sensitive to the protons inside nucleus regardless of the neutron distribution. Alternatively, the electron scattering cannot be applied for the neutron spectroscopy. Complete Distorted Wave Impulse Approximation (CDWIA), in which the Coulomb distortion of the electron wave functions in addition to the proton distorted waves are used, is applied for the analysis [33].

It is currently impossible to apply this reaction for the study of unstable isotopes because no static electron target exists. If the intensity of the radioactive beam is much increased and the collision to the electron beam is realized, then this technique will be available also for unstable isotopes.

One-nucleon removal from heavy-ion beam

The one-nucleon removal from the intermediate- and high-energy projectile beams have been used to obtain the single-particle strength in nuclei [34]. Usually the energies of γ rays measured in coincidence are used to identify the excited state of the residual nucleus. The orbital angular

momentum l is determined from the longitudinal momentum distribution. The reaction is analyzed with eikonal and sudden approximation [35, 36]. Gade *et al.* claim the model dependence is less than that for transfer reactions which are free from the dependence coming from the optical potentials and bound-state potentials. As shown in the previous section, the reduction factor R_s of 0.6–0.7 is reproduced for stable nuclei while R_s for nuclei far from β-stability has strong dependence on the proton/neutron binding energy difference [12].

The nucleon knockout reaction

The quasi-free (p, pN) scattering at high-energy >100 MeV is also used as a spectroscopic tool [37, 38] for the single-hole states in nuclei. At the high energy, this reaction can be understood as a simple single-step process. A nucleon is struck out by a nucleon and the residual nuclei is left as a spectator. The reaction analyses are carried out with the distorted wave impulse approximation (DWIA) method. Increased degree of freedom of three-body kinematics offers the determination of the Fermi momentum, *i.e.* the momentum which the struck nucleon had in the bound nucleus. It can be determined from the measured momenta of two scattered nucleons. In addition, model independent determination of total angular momentum J is capable with the use of polarized protons [39, 40] by measuring A_y in similar way as transfer reactions.

With this reaction, one can probe a more inner part of nuclei than with transfer reactions or with nucleon removal by heavy-ion. Therefore this reaction is suited to the investigation of single-particle wave functions.

More details of this method are described in Chapter 2.

1.4 Scope of this work

The purpose of this thesis is to discuss how the spin-orbit splitting and the reduction of single-particle strength change in oxygen isotopes as the change of neutron number. To investigate this correlation, we chose the oxygen isotopes as the most suitable target. The essential point is that one can obtain all the oxygen isotopes from the proton drip-line (^{13}O) to the proton drip-line (^{24}O) at the RIKEN RI Beam Factory (RIBF). Therefore one can reach the extreme area in the $R_s - \Delta S$ correlation plot in a systematic measurement of an isotopic chain. ΔS is -18.55 MeV for ^{14}O and 22.92 MeV for ^{24}O, and they will be plotted in Fig. 1.2 in the extremely left (^{14}O) and right (^{24}O) areas.

Both of two goals requires the information of the spectroscopic factor for each state. In order to obtain the spectroscopic factors, the exclusive measurement of the cross section of O$(p, 2p)$ reaction was performed.

The experiment was carried out at the SHARAQ beam line at RIKEN RIBF. The primary beam was ^{48}Ca at ~250 MeV/nucleon with typical intensity of ~100 pnA. The secondary beams of oxygen unstable isotopes were produced through the fragmentation reaction on ^{9}Be and selected by BigRIPS fragment separator. The secondary beam bombarded the solid polarized proton target. The momenta of the two scattered protons were measured by using two detector set consisting of multi-wire drift chambers (MWDC) and plastic scintillators. The residual nuclei were analyzed by using the SHARAQ magnets SDQ and D1. The detail of the experimental setup is described in Chapter 3. The $(p, 2p)$ proton-knockout event was selected by the particle identification of both of two scattered particles and the residual nucleus. The proton separation energy and the excitation energy of the residual nitrogen isotopes was calculated

from the momenta of two scattered protons. In Chapter 4, the detail of the analysis procedure is described.

The spectroscopic factors of the ground states and the low-lying excited states were determined by comparing the experimental cross section to the cross section obtained by DWIA calculations with two kinds of optical models. Then the spin-orbit splitting for ^{14}O was deduced. The details are written in Chapter 5.

The polarized observables such as absolute polarization of the target and the analyzing power of the reaction will not be treated in this thesis.

1.5 Contribution by the author

In the present work, the contributions of the author are as follows.

Development of the vacuum chamber for the polarized target

The author developed a new vacuum chamber for the polarized target because the old one has too small windows to carry out the $(p, 2p)$ reaction measurement. This development was necessary to perform the large acceptance measurement of the $(p, 2p)$ reaction with the polarized target.

Preparation of the experiment

Since there had been no precedent experiment of the exclusive measurement of the $(p, 2p)$ reaction with the polarized target, the author prepared a simulation code for the calculation of cross section and analyzing power to determine the optimal experimental conditions. The author fully organized the preparation work for the SHARAQ04 experiment.

Data reduction

All the data reduction was fully done by the author. The author developed all the analysis routines used in the data reduction, which are written in C++ with ARTEMIS [41] libraries based on the ROOT analysis framework [42]. They are well-equipped for the re-utilization in the analysis of future experiments with various detector setups. The author is also a contributor of the ARTEMIS develop team.

Reaction analysis

The reaction analysis by using a computer code THREEDEE was done by the author. It covers from the consideration of calculation parameter to the inspection inside the THREEDEE code. The calculation framework used for the transformation of the kinematics, the integration of the differential cross section, and the deduction of the momentum distribution in the acceptance of the inverse kinematics measurement was developed from scratch by the author.

Chapter 2

Quasi-free Proton Knockout Reaction

In the present work, we used the quasi-free proton knockout reaction on oxygen unstable isotopes to study their proton single-particle orbits. In this chapter, the characteristics of the quasi-free proton knockout reaction will be described.

2.1 Overview

The quasi-free nucleon knockout reaction is recognized as a powerful spectroscopic tool from the late 1950's for the investigation of the shell model of atomic nuclei. It has a strong selectivity to populate the single-nucleon hole states and therefore the proton separation energies and the orbital angular momenta of the hole states in a wide range of stable isotopes have been obtained from this reaction.

Figure 2.1 shows the energy spectrum and the angular correlations of the ^{6}Li$(p,2p)^{5}$He reaction. In the left panel, two peaks corresponding to 0p (proton separation energy $S \sim 4.8$ MeV) and 0s hole-state ($S \sim 22.4$ MeV) are well separated. The angular distribution of the differential cross section for the p state (right panel) and that for the s state (middle panel) have a clear difference depending on the orbital angular momenta of the populated hole states.

By this means, the energies and the angular momenta of single hole states have been systematically studied. Figure 2.2 shows the separation energies and angular momentum assignments of the hole states obtained from the systematic measurements of the quasi-free scattering. The increasing tendency of separation energies of the hole states for each angular momentum has been a strong basis for the verification of the nuclear shell model.

As the development of the spectrometer equipment and the polarized proton beam, the measurement of the $(p,2p)$ reaction in normal kinematics has been much sophisticated. Figure 2.3 shows the spectra of the ^{40}Ca$(\vec{p},2p)$ reaction at an energy of 200 MeV/u [43, 44] measured with two spectrometers in Research Center for Nuclear Physics (RCNP), Osaka University. A very high resolution of $\sim$ 200 keV and the extremely clean reaction mechanism enabled the observation of the fine structure of single-hole states which cannot be seen before. In addition, the utilization of the spin-polarization ($\vec{p}$ indicates that the injected proton is spin-polarized) realized the determination of total angular momentum J for fragmented states in highly excited region. With the multipole decomposition analysis method, J information can be extracted even for the continuum state [43, 44]. See Appendix A for the spin asymmetry and the J determination with this reaction.

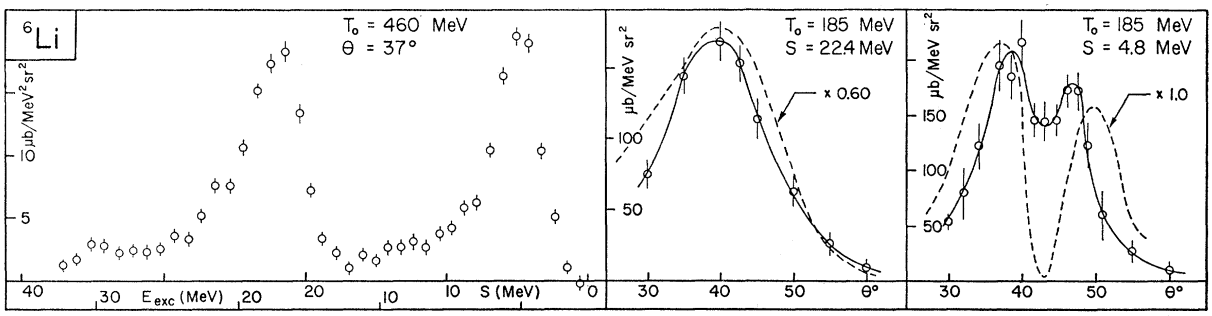

Figure 2.1: Energy spectrum and angular correlations of the differential cross section for ^{6}Li$(p, 2p)^5$He. (quoted from Ref. [37])

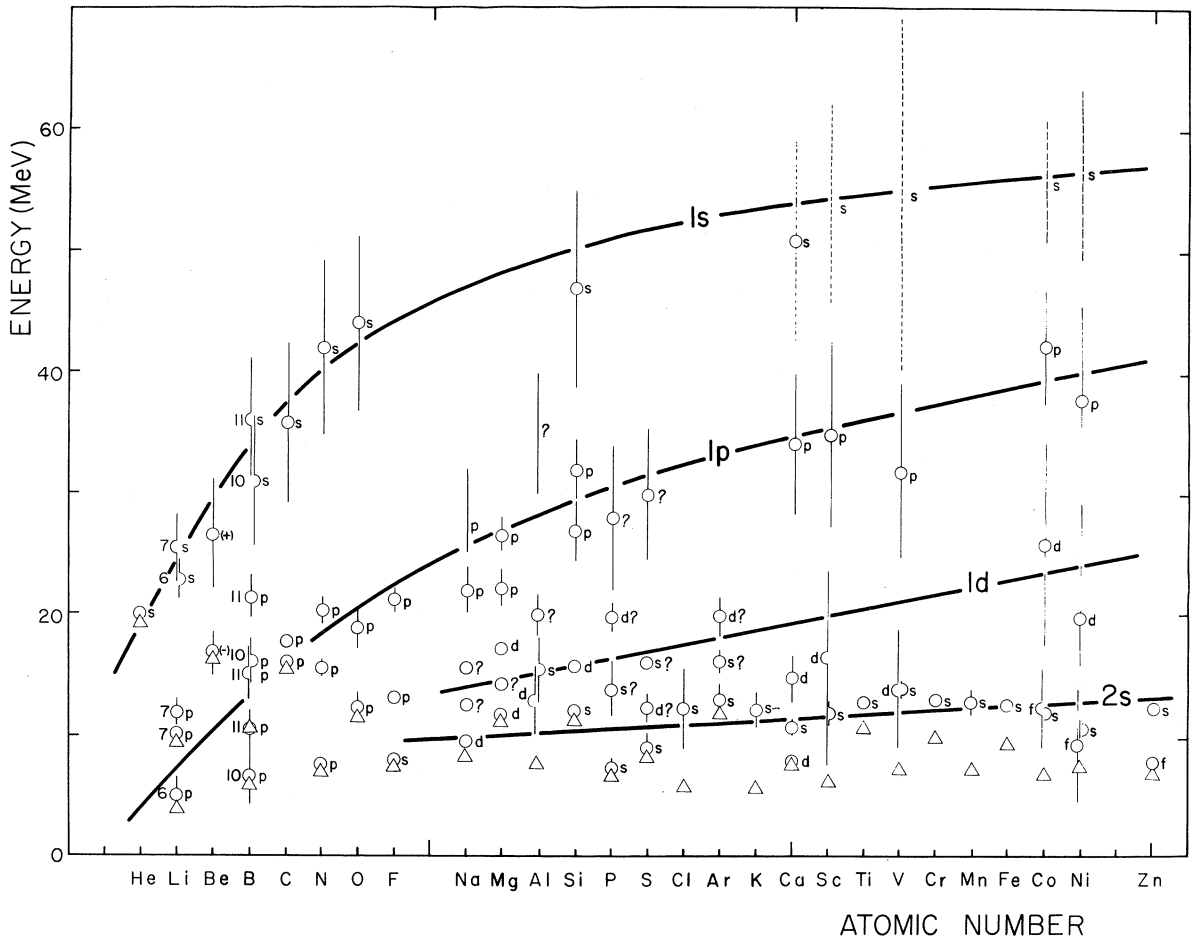

Figure 2.2: Separation energies and angular momentum assignments of the hole states obtained from quasi-free scattering. (quoted from Ref. [38])

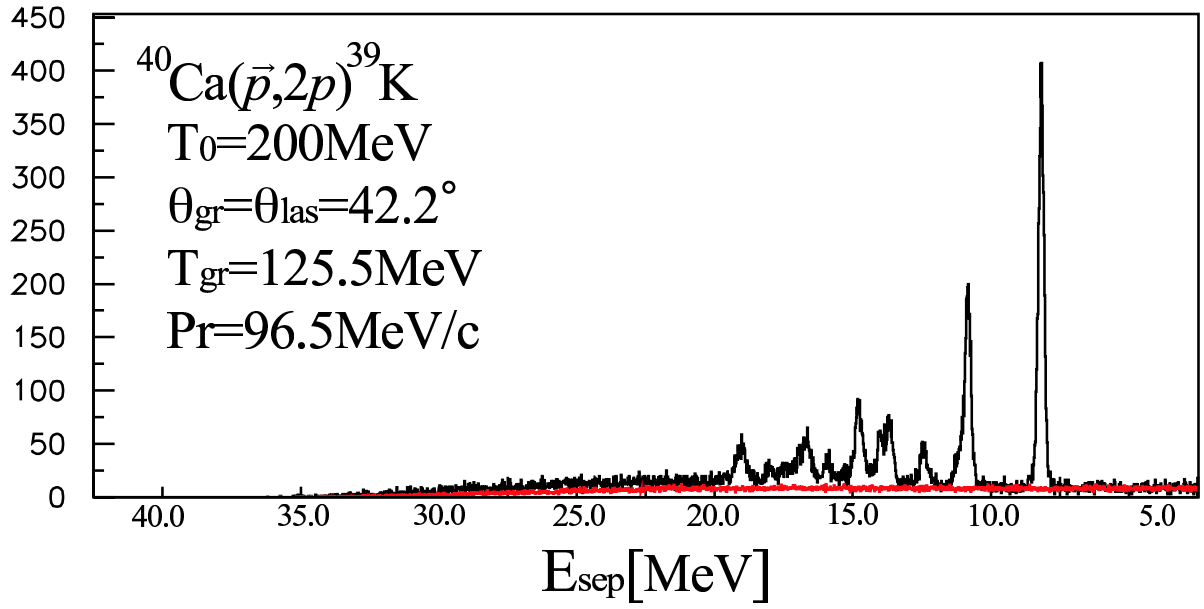

Figure 2.3: Separation energy spectrum of the ^{40}Ca($\vec{p}$, 2p) reaction. The red line shows the background spectrum. (quoted from Ref. [43])

2.2 The (p, 2p) reaction at intermediate energy

The quasi-free nucleon knockout reaction at intermediate energies above ~200 MeV/u is a powerful spectroscopic tool for the study of single-hole states in atomic nuclei [37, 38]. In this reaction, the single-step direct process is dominant [44] as well as in the (e, $e'p$) reaction [45] and therefore it selectively populates nucleon single-hole states and leave no significant disturbance on the residual nucleus. This nature leads to the reasonable reaction analysis on the basis of the distorted wave impulse approximation (DWIA).

The big advantage of this reaction is that it has a relatively larger cross section in the intermediate energy region compared to other probes used for single-particle/hole states such as transfer reactions. It is due to the absence of the momentum matching condition and somewhat longer mean-free path of nucleons inside nuclei originating from the high NN transparency at this energy region. Figure 2.4 shows the kinetic energy dependence of the NN total cross section σ_{NN}. The NN system becomes most transparent in the energy region of several hundred MeV. The total cross section monotonically reduces as the kinetic energy grows up to ~ 300 MeV, but the reaction cross section increases in the higher energy region. It is mainly due to the pion production reactions such as $p + p \rightarrow p + p + \pi^0$ and $p + p \rightarrow p + n + \pi^+$. Their thresholds are at around 280 MeV.

There is another merit if this reaction is applied to the study of unstable isotopes which inevitably requires inverse kinematics measurement. In inverse kinematics, the exclusive measurement of the reaction with small momentum transfer such as transfer reactions is rather difficult because the recoil particle has a low kinetic energy in the laboratory system and is easily stopped in the reaction target. On the other hand, the quasi-free scattering has a larger momentum transfer and the scattered nucleons have large kinetic energies. This feature makes the exclusive measurement of the reaction relatively easy.

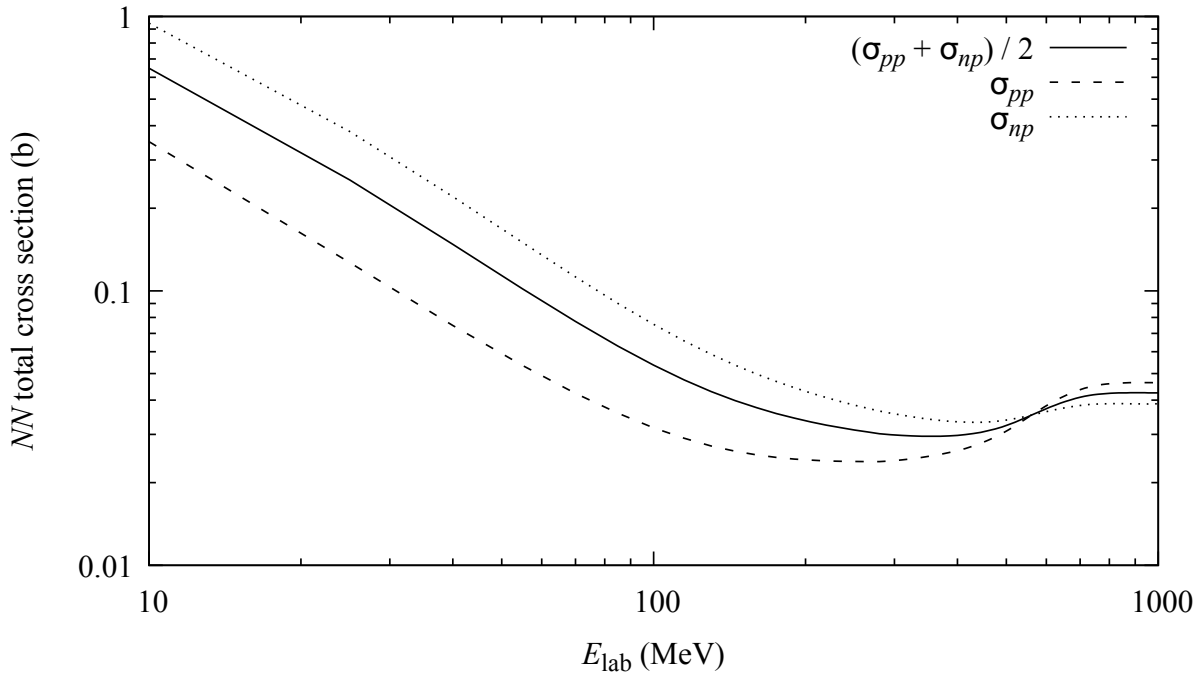

Figure 2.4: Energy dependence of the *NN* total cross sections. The cross section values are taken from the SAID database [46]. In the energy region of 200–500 MeV, *NN* system becomes most transparent and thus one can study most inner part of nuclei by using nucleon probes.

2.3 Kinematics

As shown in the previous section, the $(p, 2p)$ reaction in the intermediate energy region can be understood as a direct knockout of a proton from the nucleus by injected one. Figure 2.5 shows a schematic view of this reaction. A proton inside a nucleus is knocked out by the injected proton and as a result, a single-hole state is populated. Due to the effect of proton absorption inside nucleus, this reaction tends to take place more in the surface region than in the inner region of the nucleus.

Provided that the target nucleus is at rest and the momentum of the injected proton is known, the kinematics has six degrees of freedom that can be represented in two ways: $\{\vec{k}, S_p, \theta_{NN}, \phi_{NN}\}$ or $\{\vec{p}_1, \vec{p}_2\}$. Here $\vec{k}$ is the missing momentum, S_p is the separation energy of the proton, θ_{NN}, ϕ_{NN} are the scattering angles in the two-nucleon (*NN*) center of mass system, and $\vec{p}_1, \vec{p}_2$ are the momenta of the scattered protons. If we take the impulse picture, the missing momentum $\vec{k}$ can be considered as the momentum of a will-be-knocked-out proton, or the Fermi momentum, in the nucleus. Hence if $\vec{p}_1$ and $\vec{p}_2$ were measured through the exclusive measurement, then the kinematics can be completely determined.

In normal kinematics, the proton separation energy strongly depends on the total energy of two scattered nucleons:

$$S_p \simeq E_i + m_p - (E_1 + E_2), \tag{2.1}$$

where E_i is the energy of the incident proton. This resolution is generally limited not only by the energy resolution of detectors but also by the energy straggling which stems from the multiple scattering process in the reaction target.

2.4 Determination of the orbital angular momentum

As mentioned above, the Fermi momentum of a proton in nucleus can be chosen by setting the appropriate kinematic condition. Consequently one can obtain the momentum distribution of the knocked-out proton inside nucleus by measuring with several kinematic conditions. As the momentum distribution has strong connection with the orbital angular momentum, we can determine the orbital angular momentum of the single-hole state populated through the reaction.

2.5 Description in inverse kinematics

As seen above, the $(p, 2p)$ reaction at high energy is a very effective spectroscopic tool. However, we cannot use this reaction for the study of unstable isotopes in the normal kinematics condition as just described because it is quite difficult or impossible to prepare the target made of radioactive isotopes due to its short lifetime. Even for ones with relatively longer lifetime, it is extremely difficult and expensive to treat them as a target because of their radioactivity. In this study, unstable isotopes were extracted as a fast beam and injected to a solid polarized proton target (inverse kinematics). Thus we can avoid the aforementioned difficulty with inverse kinematics measurement.

In inverse kinematics measurements, a target nucleus with high energy is induced on a proton as shown in Fig. 2.6. The most different point from the case of normal kinematics is that the residual nucleus travels at a beam-like velocity. This feature enables the identification of residual nuclei after the reaction. Although the detection of the residual nucleus is not necessary in the study of the knockout reaction, we can investigate the physical quantities in the correlation with their decay properties.

As is the case with normal kinematics, the kinematics can be completely determined from the measurement of $\vec{p}_1$ and $\vec{p}_2$. The method to obtain the physical observables is described in the following part of this section.

Hereafter, the suffixes $_{0,1,2,T,R}$ indicate the scattered protons (1 and 2), target nuclei, and residual nuclei, respectively. The observables in the laboratory frame (LF) and the beam-rest frame (BF) are indicated without and with primes except for $\boldsymbol{k}$ (e.g. E_1 is the energy of the 1st scattered proton in LF and E'_1 is that in BF).

To begin with, let's assume the kinematics in BF. The conservation law of energy in BF is

$$E'_0 + E'_T = E'_1 + E'_2 + E'_R \tag{2.2}$$

$$\Leftrightarrow \quad m_p + T'_0 + m_T = 2m_p + T'_1 + T'_2 + m_R + T'_R \tag{2.3}$$

$$\Leftrightarrow \quad m_p + m_R - m_T = T'_0 - T'_1 - T'_2 - T'_R. \tag{2.4}$$

Separation energy can be defined as the difference of sum of masses between before and after the reaction. Therefore,

$$\begin{aligned} S_p &:= (2m_p + m_R) - (m_p + m_T) \\ &= m_p + m_R - m_T \\ &= T'_0 - T'_1 - T'_2 - T'_R \\ &= T'_0 - T'_1 - T'_2 - \frac{k^2}{2m_R}. \end{aligned} \tag{2.5}$$

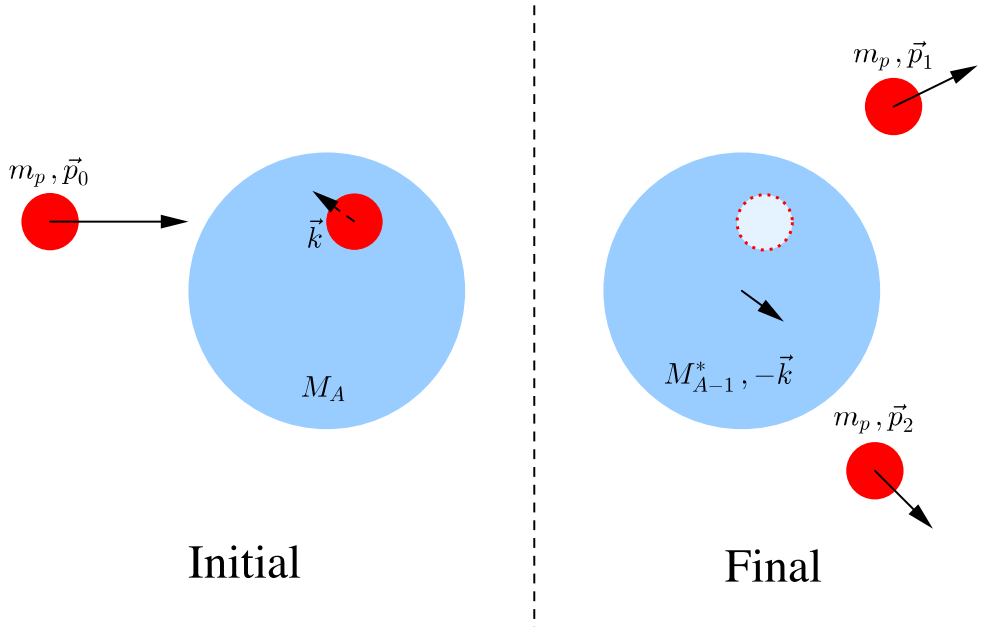

Figure 2.5: Schematic view of the $(p, 2p)$ reaction in normal kinematics. A proton is knocked out from the nucleus by an injected proton with high energy.

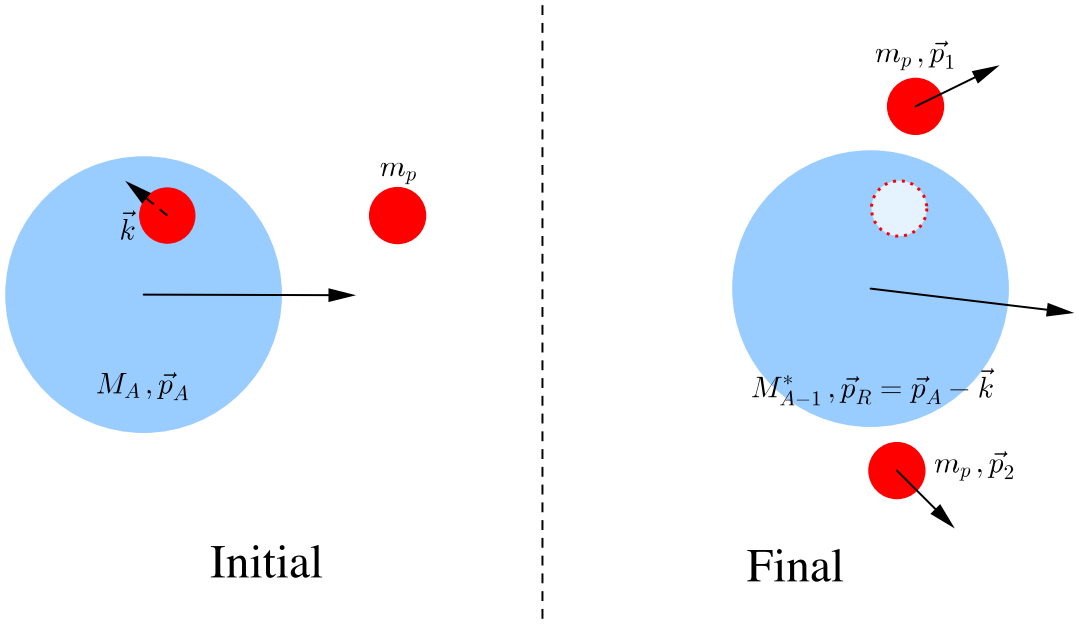

Figure 2.6: Schematic view of the $(p, 2p)$ reaction in inverse kinematics. In contrast to normal kinematics, the residual nucleus travels in very forward angle after the reaction.

Since we can directly measure the observables only in LF, Eq. (2.5) should be represented by using the observables in LF by Lorentz transformation from LF to BF:

$$E' = \gamma\left(E - \beta p_{\parallel}\right) \tag{2.6}$$

$$\Leftrightarrow T' = (\gamma - 1)m + \gamma\left(T - \beta p_{\parallel}\right), \tag{2.7}$$

where $\gamma = \left(1 - \beta^2\right)^{-1/2} = E_T/m_T$. By using this,

$$\begin{aligned} S_p &= T'_0 - T'_1 - T'_2 - \frac{k^2}{2m_R} \\ &= (\gamma - 1)m_p - (\gamma - 1)m_p - \gamma\left(T_1 - \beta p_{1\parallel}\right) - (\gamma - 1)m_p - \gamma\left(T_2 - \beta p_{2\parallel}\right) - \frac{k^2}{2m_R} \\ &= (1 - \gamma)\, m_p - \gamma\,(T_1 + T_2) + \beta\gamma\left(p_{1\parallel} + p_{2\parallel}\right) - \frac{k^2}{2m_R}. \end{aligned} \tag{2.8}$$

k^2 can also be represented by using LF observables. The conservation law of momentum in BF is

$$\begin{aligned} \boldsymbol{p}'_0 + \boldsymbol{p}'_T &= \boldsymbol{p}'_1 + \boldsymbol{p}'_2 + \boldsymbol{p}'_R \\ \Leftrightarrow \qquad \boldsymbol{k} &= \boldsymbol{p}'_1 + \boldsymbol{p}'_2 - \boldsymbol{p}'_0. \end{aligned} \tag{2.9}$$

By using Lorentz transformation of momentum from BF to LF

$$p_{\perp} = p'_{\perp}, \tag{2.10}$$

$$\begin{aligned} p_{\parallel} &= \gamma\left(p'_{\parallel} + \beta E'\right) \\ \Leftrightarrow p'_{\parallel} &= \gamma^{-1} p_{\parallel} - \beta E', \end{aligned} \tag{2.11}$$

the components of $\boldsymbol{k}$ can be represented as

$$k_{\perp} = p_{1\perp} + p_{2\perp}, \tag{2.12}$$

and

$$\begin{aligned} k_{\parallel} &= p'_{1\parallel} + p'_{2\parallel} - p'_{0\parallel} \\ &= \gamma^{-1}\left(p_{1\parallel} + p_{2\parallel} - p_{0\parallel}\right) - \beta\left(E'_1 + E'_2 - E'_0\right) \\ &= \gamma^{-1}\left(p_{1\parallel} + p_{2\parallel}\right) - \beta\left(m_T - m_R - \frac{k^2}{2m_R}\right). \end{aligned} \tag{2.13}$$

Since $k_{\parallel}$ includes itself implicitly in the last term, iterative method is needed to the calculation of k^2. The $k^2/2m_R$ term is not negligible. For example, in ^{14}O case, $m_R \simeq 13$ GeV and $k \simeq 100$ MeV/c. Therefore $k^2/2m_R \simeq 0.4$ MeV.

The description of physical quantities in inverse kinematics has a kind of duality relationship to those in normal kinematics. Table 2.1 shows the most essential experimental observable for each physical quantity in normal and inverse kinematics. For example, the magnitude of the proton separation energy is strongly reflected in the opening angle $\Delta\theta = \theta_1 - \theta_2$ in the inverse kinematics measurement.

Table 2.1: Essential experimental observables for the determination of physical quantities in normal and inverse kinematics.

	Normal kinematics	Inverse kinematics
S_p	$E_1 + E_2$	$\theta_1 - \theta_2$
$k_\parallel$	$\theta_1 - \theta_2$	$E_1 + E_2$
$k_\perp$	$E_1 - E_2$	$E_1 - E_2$

2.6 Consideration of the beam energy in the experiment

The present experiment was proposed to measure the spin asymmetry of the $(\vec{p}, 2p)$ reaction in order to determine the spin-orbit splitting of 0p proton orbits in oxygen unstable isotopes. For this purpose, the intermediate energy around 250 MeV/u is the most appropriate because the spin correlation coefficient C_{yy} for the free NN scattering in this energy region becomes very large in wide region of the scattering angle and it results in the large spin asymmetry.[1]

[1]However, the analysis on polarized observables will not be treated in this paper because of short of the statistics in the present experiment. For the detail mechanism of the spin asymmetry of the $(\vec{p}, 2p)$ reaction, see Appendix A.

Chapter 3

Experiment

本章については、5年以内に雑誌等で刊行予定のため、非公開。

Chapter 4

Data Analysis

本章については、5年以内に雑誌等で刊行予定のため、非公開。

Chapter 5

Discussion

本章については、5年以内に雑誌等で刊行予定のため、非公開。

Chapter 6

Conclusion

本章については、5年以内に雑誌等で刊行予定のため、非公開。

Acknowledgments

I would like to express my profound gratitude to Dr. Tomohiro Uesaka, who was my supervisor and introduced me this interesting and exciting field of study. Discussions with him were always stimulating and made me a lot of help. Without his sincere and persistent encouragement, this study would not be completed.

My heartfelt appreciation goes also to Prof. Susumu Shimoura, who is my supervisor in PhD course, for his constant encouragement. I have been often inspired by his ideas and suggestions based on his keen insight into physics.

I would like to offer my special thanks to Dr. Shinsuke Ota. Advice and comments given by him has been an enormous help to me and I also received generous support from him. Besides, his launch of the development of ARTEMIS code saved me when I was almost giving up the analysis.

I am deeply grateful particularly to Dr. Masaki Sasano. I learned the importance of the scrupulousness from him through the preparation of the experiment. His astute comments were invaluable for me.

Discussions on the theoretical models for the $(p, 2p)$ reaction with Prof. Kazuyuki Ogata have been highly illuminating. The calculation codes for the density distribution and the folded potential were also provided from him. The face-to-face discussion with him and his colleagues Dr. Kosho Minomo and Mr. Kazuki Yoshida was especially exciting.

Special thanks go to the collaborators of SHARAQ04 experiment: Mr. Tsz Leung Tang, Dr. Tomohiro Uesaka, Prof. Didier Beaumel, Dr. Masanori Dozono, Mr. Toshihiko Fujii, Dr. Naoki Fukuda, Prof. Alfredo Galindo-Uribarri, Dr. Sanghoon Hwang, Dr. Naoto Inabe, Dr. Daisuke Kameda, Dr. Tomomi Kawahara, Prof. Wooyoung Kim, Dr. Keiichi Kisamori, Mr. Motoki Kobayashi, Dr. Toshiyuki Kubo, Mr. Yuki Kubota, Dr. Kensuke Kusaka, Mr. Cheongsoo Lee, Prof. Yukie Maeda, Dr. Hiroaki Matsubara, Dr. Shin'ichiro Michimasa, Mr. Hiroyuki Miya, Prof. Tetsuo Noro, Prof. Alexandre Obertelli, Dr. Shinsuke Ota, Dr. Elizabeth Padilla-Rodal, Dr. Satoshi Sakaguchi, Dr. Hideyuki Sakai, Dr. Masaki Sasano, Prof. Susumu Shimoura, Dr. Samvel Stepanyan, Dr. Hiroshi Suzuki, Mr. Motonobu Takaki, Dr. Hiroyuki Takeda, Mr. Hiroshi Tokieda, Dr. Takashi Wakui, Prof. Kentaro Yako, Mr. Jumpei Yasuda, Dr. Yoshiyuki Yanagisawa, Mr. Rin Yokoyama, Dr. Koichi Yoshida, and Dr. Juzo Zenihiro for their valuable contributions. I also appreciate the accelerator staff of the RIKEN Nishina Center for providing high-quality oxygen beams.

I would like to thank Imai Shinku Co., Ltd. for the production of the complex target chamber with their experienced craftsmanship.

This work was financially supported by a Grant-in-Aid for Japan Society for the Promotion of Science (JPS) Fellows (No. $23 \cdot 6202$).

I wish to thank the present and past members of Center for Nuclear Study, the University of Tokyo. I really enjoyed the life being there for six years.

I owe a very important debt to Prof. Yukinobu Watanabe and Dr. Hideaki Otsu for offering a

job opportunity at Kyushu University. With their permissiveness and constant encouragement, I could have completed this dissertation in parallel with the daily work.

I would also like to thank to the members of the thesis committee, Prof. Hidetoshi Yamaguchi, Prof. Takaharu Otsuka, Prof. Sachio Komamiya, Prof. Noritaka Shimizu, and Prof. Wataru Otani for their invaluable advice and comments.

Last, but not least, my cordial gratitude goes to my parents for their unconditional encouragement and support over years, and to my wife, Mizuki, for all her love and understanding.

Appendix A

Spin Asymmetry of the $(p, 2p)$ Reaction

The spin-parity (J^π) of the state can be determined by the strong J^π dependences of the cross section and the analyzing power of the $(\vec{p}, 2p)$ reaction. In energy region of 200–300 MeV, it is known that the spin-up proton is more likely to react with spin-up protons than with spin-down ones. Figure A.1 shows the spin correlation coefficient $C_{y,y}$ for the proton-proton scattering. Positive $C_{y,y}$ indicates that scattering occurs mostly for spin-parallel protons and negative $C_{y,y}$ for spin-antiparallel protons. This fact leads the J^π dependence of the $(\vec{p}, 2p)$ reaction (Maris effect [40]).

For example, if a proton with spin-up is injected, it is likely to react with spin-up protons in the nucleus for aforementioned reasons. There are two possible total angular momentum for a given orbital angular momentum l. One has the total angular momentum $j_> = l + 1/2$, and the other $j_< = l - 1/2$. From a classical perspective, they revolve in the opposite direction in the nucleus as shown in Fig. A.2. Assume the kinematics of a head-on collision with the resulted lower-energy proton scattered to the right as in Fig. A.2. In the scattering with a $j_>$ proton (Case (a) in Fig. A.2), the low energy proton has to travel a longer path in nucleus than in the scattering with a $j_<$ proton (Case (b)). Since the mean free path is shorter for low energy protons, a longer path in nucleus increases the reabsorption probability of the low energy proton and hence reduces the differential cross section of the $(p, 2p)$ reaction. Thus, the spin asymmetry appears. One can determine the J^π value from the measurement of the spin asymmetry, or vector analyzing power A_y, in combination with the cross section. Here A_y is defined as

$$A_y = \frac{1}{P} \frac{\sigma_\uparrow - \sigma_\downarrow}{\sigma_\uparrow + \sigma_\downarrow}, \tag{A.1}$$

where P is the proton polarization and $\sigma_{\uparrow(\downarrow)}$ is the (differential) cross section of the reaction with spin-up (spin-down) beam.

It is empirically known that the difference of the analyzing power for the spin doublet becomes large when the scattered angles of two protons are set to the same angle. Figure A.3 shows the differential cross section and the analyzing power for the $^{16}\mathrm{O}(\vec{p}, 2p)$ reaction at an incident energy of 200 MeV corresponding to the $0\mathrm{p}_{1/2}$ and the $0\mathrm{p}_{3/2}$ proton knockout measured by Kitching *et al.* [111]. The scattering angles of two protons were set to 30°. The analyzing powers for the $0\mathrm{p}_{1/2}$ and the $0\mathrm{p}_{3/2}$ proton knockout have opposite sign and a large difference between them. Thus one can easily identify the J^π values of the discrete states from the momentum dependence of the cross section and the analyzing power.

This method can be applied also to the strengths in the continuum region. The strengths are decomposed into contributions from different orbits by the multipole decomposition analysis (MDA) [44, 43].

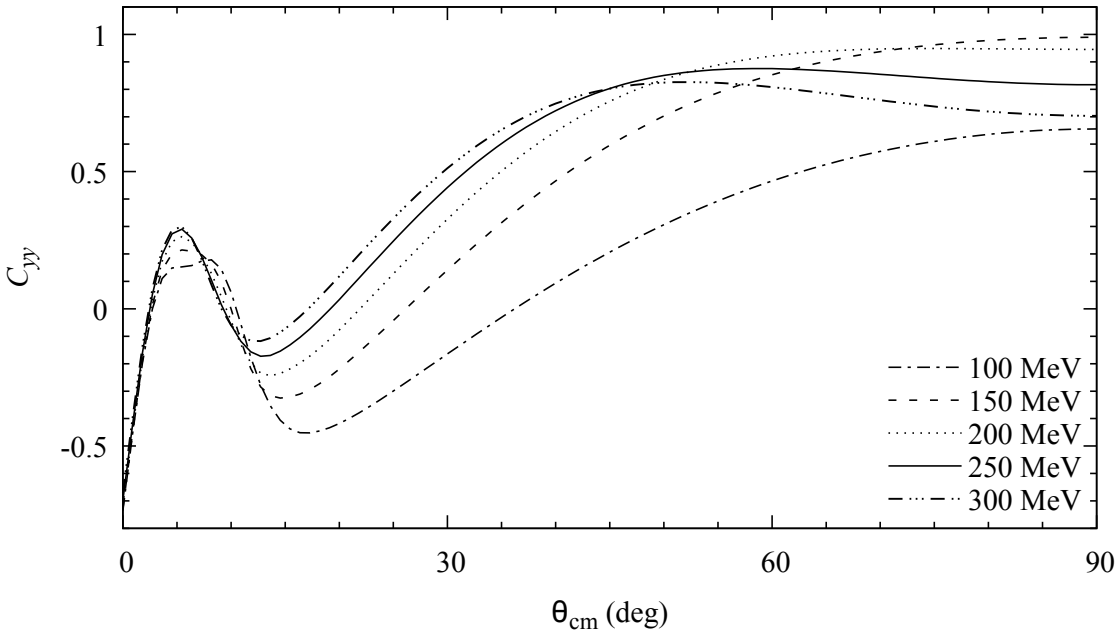

Figure A.1: Spin correlation coefficient $C_{y,y}$ for the pp scattering for several kinetic energies in the laboratory system. θ_{cm} is the scattering angle in the center-of-mass system. Large positive/negative $C_{y,y}$ indicates that the spin-parallel/antiparallel coupling is favorable.

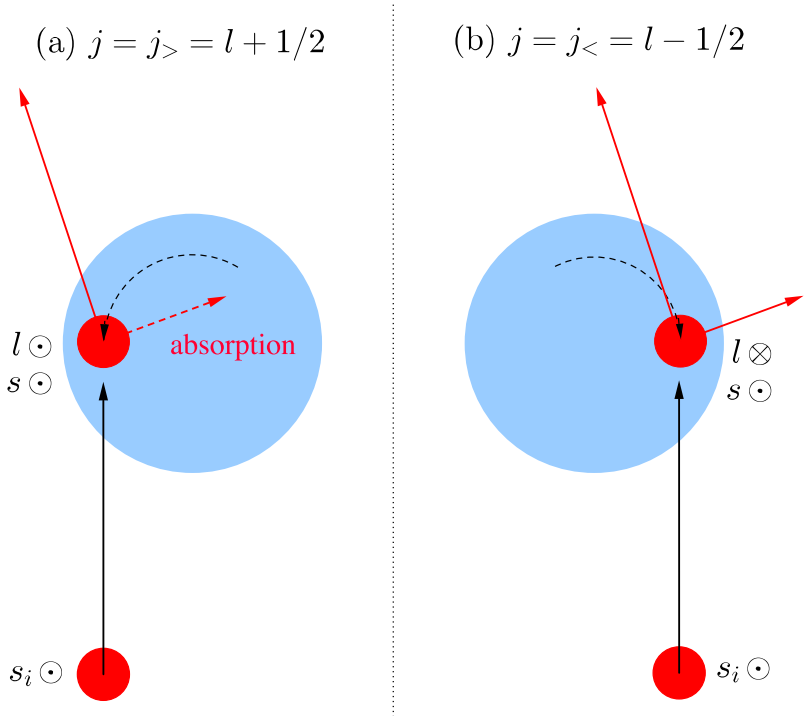

Figure A.2: J^π dependence of the $(\vec{p}, 2p)$ reaction. In this case, the traversing path of the proton with low energy, which will be scattered to the right, is longer in the scattering with the $j_>$ proton (Case (a)) than in that with the $j_<$ proton (Case (b)). The difference of the traversing paths results in that of the differential cross sections and therefore the J^π dependence appears.

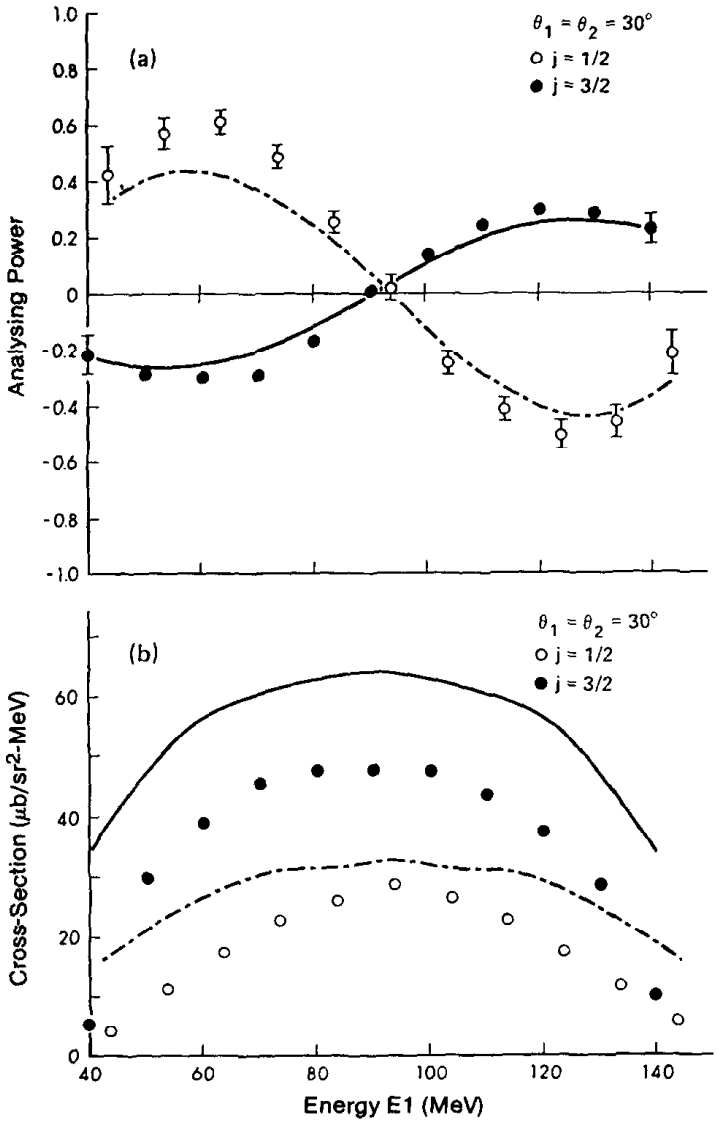

Figure A.3: Differential cross section and analyzing power for the $^{16}O(\vec{p}, 2p)$ reaction measured by Kitching *et al.* [111]. The abscissa is the kinetic energy of one of the final-state protons.

Appendix B

Transformation of the Differential Cross Section

Consider to calculate the differential cross section in inverse kinematics from that in normal kinematics.

$$\frac{d^3\sigma}{dE_1 d\Omega_1 d\Omega_2} = \left|\frac{\partial(E_1', \Omega_1', \Omega_2')}{\partial(E_1, \Omega_1, \Omega_2)}\right| \cdot \frac{d^3\sigma}{dE_1' d\Omega_1' d\Omega_2'} \tag{B.1}$$

$$= \left|\frac{\partial(E_1', \Omega_1')}{\partial(E_1, \Omega_1)}\right| \left|\frac{\partial(\Omega_2')}{\partial(\Omega_2)}\right| \cdot \frac{d^3\sigma}{dE_1' d\Omega_1' d\Omega_2'}. \tag{B.2}$$

Firstly, let's consider the general case. Assume the transformation between the n-dimensional spaces $(x_0, \cdots, x_n)$ and $(y_0, \cdots, y_n)$ which can be represented by using differentiable vector functions A_i and B_i as follows:

$$A_i(x_0, \cdots, x_n) = B_i(y_0, \cdots, y_n). \tag{B.3}$$

$\frac{\partial y_i}{\partial x_j}$ is obtained by operating $\frac{\partial}{\partial x_j}$ on the both side of Eq. (B.3):

$$\frac{\partial A_i}{\partial x_j} = \frac{\partial B_i}{\partial x_j} \tag{B.4}$$

$$\Leftrightarrow \frac{\partial A_i}{\partial x_j} = \sum_k \frac{\partial B_i}{\partial y_k}\frac{\partial y_k}{\partial x_j}. \tag{B.5}$$

In matrix form,

$$P = QJ, \tag{B.6}$$

where

$$P_{ij} = \frac{\partial A_i}{\partial x_j}, Q_{ij} = \frac{\partial B_i}{\partial y_j}, \text{ and } J_{ij} = \frac{\partial y_i}{\partial x_j}. \tag{B.7}$$

If Q is a regular matrix, Jacobian matrix J can be obtained as follows:

$$J = Q^{-1}P. \tag{B.8}$$

The transformation from normal to inverse kinematics can be represented in the following equations:

$$p' \cos\theta' = \gamma\beta E + \gamma p \cos\theta, \tag{B.9}$$

$$p' \sin\theta' \cos\phi' = p \sin\theta \cos\phi, \tag{B.10}$$

$$p' \sin\theta' \sin\phi' = p \sin\theta \sin\phi. \tag{B.11}$$

In this case,

$$J = \begin{pmatrix} \dfrac{\partial E'}{\partial E} & \dfrac{\partial E'}{\partial \cos\theta} & \dfrac{\partial E'}{\partial \phi} \\ \dfrac{\partial \cos\theta'}{\partial E} & \dfrac{\partial \cos\theta'}{\partial \cos\theta} & \dfrac{\partial \cos\theta'}{\partial \phi} \\ \dfrac{\partial \phi'}{\partial E} & \dfrac{\partial \phi'}{\partial \cos\theta} & \dfrac{\partial \phi'}{\partial \phi} \end{pmatrix}, \tag{B.12}$$

$$P = \begin{pmatrix} \gamma\beta + \dfrac{\gamma E \cos\theta}{p} & \gamma p & 0 \\ \dfrac{E}{p} \sin\theta \cos\phi & -p \cot\theta \cos\phi & -p \sin\theta \sin\phi \\ \dfrac{E}{p} \sin\theta \sin\phi & -p \cot\theta \sin\phi & p \sin\theta \cos\phi \end{pmatrix}, \tag{B.13}$$

$$\text{and } Q = \begin{pmatrix} \dfrac{E'}{p'} \cos\theta' & p' & 0 \\ \dfrac{E'}{p'} \sin\theta' \cos\phi' & -p' \cot\theta' \cos\phi' & -p' \sin\theta' \sin\phi' \\ \dfrac{E'}{p'} \sin\theta' \sin\phi' & -p' \cot\theta' \sin\phi' & p' \sin\theta' \cos\phi' \end{pmatrix}. \tag{B.14}$$

The determinants are

$$\det P = -E' p, \tag{B.15}$$

$$\det Q = -E' p'. \tag{B.16}$$

This $\det Q$ vanishes if and only if $p' = 0$. $p' = 0$ means the scattered nucleon was completely stopped after the scattering and it will never be detected. Thus Q^{-1} exists whenever the scattered nucleon is detected. Therefore,

$$\det J = \det Q^{-1} \cdot \det P \tag{B.17}$$

$$= (\det Q)^{-1} \cdot \det P \tag{B.18}$$

$$= \frac{p}{p'}, \tag{B.19}$$

$$Q^{-1} = \frac{1}{E' p'} \begin{pmatrix} p'^2 \cos\theta' & p'^2 \sin\theta' \cos\phi' & p'^2 \sin\theta' \sin\phi' \\ E' \sin^2\theta' & -E' \cos\theta' \sin\theta' \cos\phi' & -E' \cos\theta' \sin\theta' \sin\phi' \\ 0 & -\dfrac{E' \sin\phi'}{\sin\theta'} & \dfrac{E' \cos\phi'}{\sin\theta'} \end{pmatrix}. \tag{B.20}$$

By using Eq. (B.8), (B.12), (B.13), and (B.20), matrix elements of J can be determined as follows:

$$\frac{\partial E'}{\partial E} = \frac{E p'}{E' p} \left[\gamma \cos\theta \cos\theta' + \sin\theta \sin\theta' \cos\left(\phi' - \phi\right) + \frac{\gamma\beta p}{E} \cos\theta' \right], \tag{B.21}$$

$$\frac{\partial E'}{\partial \cos\theta} = \frac{pp'}{E'}\left[\gamma\cos\theta' - \cot\theta\sin\theta'\cos\left(\phi'-\phi\right)\right], \tag{B.22}$$

$$\frac{\partial E'}{\partial \phi} = \frac{pp'}{E'}\sin\theta\sin\theta'\sin\left(\phi'-\phi\right), \tag{B.23}$$

$$\frac{\partial \cos\theta'}{\partial E} = \frac{E}{pp'}\sin\theta'\left[\gamma\cos\theta\sin\theta' - \sin\theta\cos\theta'\cos\left(\phi'-\phi\right) + \frac{\gamma\beta p}{E}\sin\theta'\right], \tag{B.24}$$

$$\frac{\partial \cos\theta'}{\partial \cos\theta} = \frac{p}{p'}\sin\theta'\left[\gamma\sin\theta' + \cot\theta\cos\theta'\cos\left(\phi'-\phi\right)\right], \tag{B.25}$$

$$\frac{\partial \cos\theta'}{\partial \phi} = -\frac{p}{p'}\sin\theta\cos\theta'\sin\theta'\sin\left(\phi'-\phi\right), \tag{B.26}$$

$$\frac{\partial \phi'}{\partial E} = -\frac{E}{pp'}\frac{\sin\theta}{\sin\theta'}\sin\left(\phi'-\phi\right), \tag{B.27}$$

$$\frac{\partial \phi'}{\partial \cos\theta} = \frac{p}{p'}\frac{\cot\theta}{\sin\theta'}\sin\left(\phi'-\phi\right), \tag{B.28}$$

$$\frac{\partial \phi'}{\partial \phi} = \frac{p}{p'}\frac{\sin\theta}{\sin\theta'}\cos\left(\phi'-\phi\right). \tag{B.29}$$

In present case, $\phi' = \phi$ can be assumed without losing any generality and then $\frac{\partial \cos\theta'}{\partial \phi}$ and $\frac{\partial \phi'}{\partial \cos\theta}$ vanish. Finally, Jacobian determinant in (B.1) is obtained by

$$\left|\frac{\partial(E_1', \Omega_1', \Omega_2')}{\partial(E_1, \Omega_1, \Omega_2)}\right| = \left|\frac{\partial(E_1', \Omega_1')}{\partial(E_1, \Omega_1)}\right|\left|\frac{\partial(\Omega_2')}{\partial(\Omega_2)}\right| \tag{B.30}$$

$$= \det J_1 \cdot \frac{\partial \cos\theta_2'}{\partial \cos\theta_2}\frac{\partial \phi_2'}{\partial \phi_2} \tag{B.31}$$

$$= \frac{p_1}{p_1'}\frac{p_2^2}{{p_2'}^2}\left(\cos\theta_2\cos\theta_2' + \gamma\sin\theta_2\sin\theta_2'\right). \tag{B.32}$$

This Jacobian determinant can be both positive and negative. This fact means that $(S, E_1, \Omega_1, \Omega_2)$ are not complete set for the specification in inverse kinematics, while $(S, E_1', \Omega_1', \Omega_2')$ are sufficient for normal kinematics: even if the separation energy (S), energy of one nucleon (E_1), and the scattering angles of two nucleons (Ω_1, Ω_2) are given, the energy of another nucleon (E_2) cannot always be uniquely determined in inverse kinematics.

Bibliography

[1] C. F. von Weizsäcker, Zeitschrift für Physik **96**, 431 (1935).

[2] H. Yukawa, Proc. Phys. Math. Soc. Jpn. **17**, 48 (1935).

[3] N. Bohr and J. A. Wheeler, Phys. Rev. **56**, 426 (1939).

[4] W. M. Elsasser, J. Phys. Radium. **5**, 635 (1934).

[5] M. G. Mayer, Phys. Rev. **75**, 1969 (1949).

[6] O. Haxel, J. H. D. Jensen, and H. E. Suess, Phys. Rev. **75**, 1766 (1949).

[7] A. Arima and H. Horie, Prog. Theor. Phys. **11**, 509 (1954).

[8] H. Horie and A. Arima, Phys. Rev. **99**, 778 (1955).

[9] V. R. Pandharipande, C. N. Papanicolas, and J. Wambach, Phys. Rev. Lett. **53**, 1133 (1984).

[10] L. Lapikás, Nucl. Phys. A **553**, 297 (1993).

[11] O. Benhar, A. Fabrocini, and S. Fantoni, Phys. Rev. C **41**, R24 (1990).

[12] A. Gade, P. Adrich, D. Bazin, M. D. Bowen, B. A. Brown, C. M. Campbell, J. M. Cook, T. Glasmacher, P. G. Hansen, K. Hosier, S. McDaniel, D. McGlinchery, A. Obertelli, K. Siwek, L. A. Riley, J. A. Tostevin, and D. Weisshaar, Phys. Rev. C **77**, 044306 (2008).

[13] J. A. Tostevin and A. Gade, Phys. Rev. C **90**, 057602 (2014).

[14] J. Lee, M. B. Tsang, D. Bazin, D. Coupland, V. Henzl, D. Henzlova, M. Kilburn, W. G. Lynch, A. M. Rogers, A. Sanetullaev, A. Signoracci, Z. Y. Sun, M. Youngs, K. Y. Chae, R. J. Charity, H. K. Cheung, M. Famiano, S. Hudan, P. O'Malley, W. A. Peters, K. Schmitt, D. Shapira, and L. G. Sobotka, Phys. Rev. Lett. **104**, 112701 (2010).

[15] F. Flavigny, A. Gillibert, L. Nalpas, A. Obertelli, N. Keeley, C. Barbieri, D. Beaumel, S. Boissinot, G. Burgunder, A. Cipollone, A. Corsi, J. Gibelin, S. Giron, J. Guillot, F. Hammache, V. Lapoux, A. Matta, E. C. Pollacco, R. Raabe, M. Rejmund, N. de Séreville, A. Shrivastava, A. Signoracci, and Y. Utsuno, Phys. Rev. Lett. **110**, 122503 (2013).

[16] I. Tanihata, Hyperfine Interactions **21**, 251.

[17] T. Motobayashi, Y. Ikeda, K. Ieki, M. Inoue, N. Iwasa, T. Kikuchi, M. Kurokawa, S. Moriya, S. Ogawa, H. Murakami, S. Shimoura, Y. Yanagisawa, T. Nakamura, Y. Watanabe, M. Ishihara, T. Teranishi, H. Okuno, and R. Casten, Phys. Lett. B **346**, 9 (1995).

[18] H. Scheit, T. Glasmacher, B. A. Brown, J. A. Brown, P. D. Cottle, P. G. Hansen, R. Harkewicz, M. Hellström, R. W. Ibbotson, J. K. Jewell, K. W. Kemper, D. J. Morrissey, M. Steiner, P. Thirolf, and M. Thoennessen, Phys. Rev. Lett. **77**, 3967 (1996).

[19] A. Ozawa, T. Kobayashi, T. Suzuki, K. Yoshida, and I. Tanihata, Phys. Rev. Lett. **84**, 5493 (2000).

[20] D. Steppenbeck, S. Takeuchi, N. Aoi, P. Doornenbal, M. Matsushita, H. Wang, H. Baba, N. Fukuda, S. Go, M. Honma, J. Lee, K. Matsui, S. Michimasa, T. Motobayashi, D. Nishimura, T. Otsuka, H. Sakurai, Y. Shiga, P.-A. Söderström, T. Sumikama, H. Suzuki, R. Taniuchi, Y. Utsuno, J. J. Valiente-Dobón, and K. Yoneda, Nature **502**, 207 (2013).

[21] K. Ando and H. Bando, Prog. Theor. Phys. **66**, 227 (1981).

[22] S. C. Pieper and V. R. Pandharipande, Phys. Rev. Lett. **70**, 2541 (1993).

[23] A. M. Feingold, Phys. Rev. **101**, 258 (1956).

[24] T. Terasawa, Prog. Theor. Phys. **23**, 87 (1960).

[25] A. Arima and T. Terasawa, Prog. Theor. Phys. **23**, 115 (1960).

[26] J. Fujita and H. Miyazawa, Prog. Theor. Phys. **17**, 360 (1957).

[27] G. Lalazissis, D. Vretenar, W. Pöschl, and P. Ring, Phys. Lett. B **418**, 7 (1998).

[28] S. Kawase, T. L. Tang, T. Uesaka, D. Beaumel, M. Dozono, T. Fujii, T. Fukunaga, N. Fukuda, A. Galindo-Uribarri, S. H. Hwang, N. Inabe, D. Kameda, T. Kawahara, W. Kim, K. Kisamori, M. Kobayashi, T. Kubo, Y. Kubota, K. Kusaka, C. S. Lee, Y. Maeda, H. Matsubara, S. Michimasa, H. Miya, T. Noro, A. Obertelli, S. Ota, E. Padilla-Rodal, S. Sakaguchi, H. Sakai, M. Sasano, S. Shimoura, S. S. Stepanyan, H. Suzuki, M. Takaki, H. Takeda, H. Tokieda, T. Wakasa, T. Wakui, K. Yako, Y. Yanagisawa, J. Yasuda, R. Yokoyama, K. Yoshida, and J. Zenihiro, JPS Conf. Proc. **6**, 020003 (2015).

[29] G. R. Satchler, *Direct Nuclear Reaction* (Oxford University Press, 1983).

[30] G. J. Kramer, H. P. Blok, and L. Lapikás, Nucl. Phys. A **679**, 267 (2001).

[31] T. Yule and W. Haeberli, Nucl. Phys. A **117**, 1 (1968).

[32] D. Brink, Phys. Lett. B **40**, 37 (1972).

[33] J. P. McDermott, Phys. Rev. Lett. **65**, 1991 (1990).

[34] B. A. Brown, P. G. Hansen, B. M. Sherrill, and J. A. Tostevin, Phys. Rev. C **65**, 061601 (2002).

[35] J. A. Tostevin, J. Phys. G **25**, 735 (1999).

[36] J. A. Tostevin, Nucl. Phys. A **682**, 320 (2001).

[37] G. Jacob and Th. A. J. Maris, Rev. Mod. Phys. **38**, 121 (1966).

[38] G. Jacob and Th. A. J. Maris, Rev. Mod. Phys. **45**, 6 (1973).

[39] G. Jacob, Th. A. J. Maris, C. Schneider, and M. R. Teodoro, Phys. Lett. B **45**, 181 (1973).

[40] G. Jacob, Th. A. J. Maris, C. Schneider, and M. R. Teodoro, Nucl. Phys. A **257**, 517 (1976).

[41] ARTEMIS: A RooT Extesion with Modular processor for Instant Swiching, https://github.com/artemis-dev/artemis.

[42] ROOT — A Data Analysis Framework, http://root.cern.ch/.

[43] Y. Nagasue, *Measurement of mean proton single particle energy in calcium isotopes via the* $(\vec{p}, 2p)$ *reaction*, Master thesis, Kyushu University, 2006.

[44] T. Noro, QFS studies at RCNP, 2008, QFS workshop at ECT, Trento.

[45] G. van der Steenhoven, H. P. Blok, E. Jans, L. Lapikás, E. N. M. Quint, and P. K. A. de Witt Huberts, Nuclear Physics A **484**, 445 (1988).

[46] The SAID Partial-Wave Analysis Facility, http://gwdac.phys.gwu.edu/.

[47] T. Wakui, M. Hatano, H. Sakai, T. Uesaka, and A. Tamii, Nucl. Instrum. Meth. A **550**, 521 (2005).

[48] Y. Yano, Nucl. Instrum. Meth. B **261**, 1009 (2007).

[49] T. Kubo, Nucl. Instrum. Meth. B **204**, 97 (2003).

[50] SHARAQ — Spectroscopy with High-resolution Analyzer of RadioActive Quantum beams, http://www.cns.s.u-tokyo.ac.jp/sharaq/.

[51] H. Okuno, J. Ohnishi, K. Yamada, N. Fukunishi, K. Ikegami, T. Maie, H. Hasebe, M. Hamanaka, M. Kase, A. Goto, and Y. Yano, IEEE Transactions on Applied Superconductivity **17**, 1063 (2007).

[52] T. Kawabata, G. P. A. Berg, T. Kubo, H. Sakai, S. Shimoura, and T. Uesaka, Nucl. Instrum. Meth. B **266**, 4201 (2008).

[53] T. Uesaka, S. Shimoura, H. Sakai, and for the SHARAQ Collaboration, Prog. Theor. Exp. Phys. **2012** (2012).

[54] H. Kumagai, A. Ozawa, N. Fukuda, K. Sümmerer, and I. Tanihata, Nucl. Instrum. Meth. A **470**, 562 (2001).

[55] H. Miya, S. Ota, T. Fujii, S. Kawase, Y. Kubota, C. S. Lee, H. Matsubara, K. Miki, A. Saito, S. Michimasa, T. Uesaka, H. Sakai, and S. Shimoura, Nucl. Instrum. Meth. B **317**, 701 (2013).

[56] H. Okamura, S. Ishida, N. Sakamoto, H. Otsu, T. Uesaka, T. Wakasa, Y. Satou, H. Sakai, T. Niizeki, H. Ohnuma, and T. Ichihara, Nucl. Instrum. Meth. A **406**, 78 (1998).

[57] H. Nishino, K. Awai, Y. Hayato, S. Nakayama, K. Okumura, M. Shiozawa, A. Takeda, K. Ishikawa, A. Minegishi, and Y. Arai, Nucl. Instrum. Meth. A **610**, 710 (2009).

[58] H. Baba, T. Ichihara, T. Ohnishi, S. Takeuchi, K. Yoshida, Y. Watanabe, S. Ota, and S. Shimoura, Nucl. Instrum. Meth. A **616**, 65 (2010).

[59] O. Tarasov and D. Bazin, Nucl. Instrum. Meth. B **266**, 4657 (2008).

[60] National nuclear data center, http://www.nndc.bnl.gov/.

[61] F. Ajzenberg-Selove, Nucl. Phys. A **523**, 1 (1991).

[62] L. Gaudefroy, W. Mittig, N. A. Orr, S. Varet, M. Chartier, P. Roussel-Chomaz, J. P. Ebran, B. Fernández-Domínguez, G. Frémont, P. Gangnant, A. Gillibert, S. Grévy, J. F. Libin, V. A. Maslov, S. Paschalis, B. Pietras, Y.-E. Penionzhkevich, C. Spitaels, and A. C. C. Villari, Phys. Rev. Lett. **109**, 202503 (2012).

[63] D. F. Jackson and T. Berggren, Nucl. Phys. **62**, 353 (1965).

[64] K. L. Lim and I. E. McCarthy, Phys. Rev. **133**, B1006 (1964).

[65] B. Jain and D. F. Jackson, Nucl. Phys. A **99**, 113 (1967).

[66] N. S. Chant and P. G. Roos, Phys. Rev. C **15**, 57 (1977).

[67] F. Perey and B. Buck, Nucl. Phys. **32**, 353 (1962).

[68] N. Austern, Phys. Rev. **137**, B752 (1965).

[69] H. Fiedeldey, Nucl. Phys. **77**, 149 (1966).

[70] L. J. Titus and F. M. Nunes, Phys. Rev. C **89**, 034609 (2014).

[71] A. Bohr and B. R. Mottelson, *Nuclear Structure I, II* (World Scientific, 1969).

[72] E. D. Cooper, S. Hama, B. C. Clark, and R. L. Mercer, Phys. Rev. C **47**, 297 (1993).

[73] K. Minomo, K. Ogata, M. Kohno, Y. R. Shimizu, and M. Yahiro, J. Phys. G **37**, 085011 (2010).

[74] F. A. Brieva and J. R. Rook, Nucl. Phys. **A 291**, 299 (1977).

[75] F. A. Brieva and J. R. Rook, Nucl. Phys. **A 291**, 317 (1977).

[76] F. A. Brieva and J. R. Rook, Nucl. Phys. **A 297**, 206 (1978).

[77] M. Toyokawa, K. Minomo, and M. Yahiro, Phys. Rev. C **88**, 054602 (2013).

[78] K. Amos, P. J. Dormans, H. V. von Geramb, S. Karataglidis, and J. Raynal, Advances in Nuclear Physics **25**, 275 (2000).

[79] R. A. Arndt, J. S. Hyslop III, and L. D. Roper, Phys. Rev. D **35**, 128 (1987).

[80] B. A. Brown, A. Etchegoyan, and W. D. M. Rae, the Oxford, Buenos-Ailes, Michigan State, Shell Model Program, MSU Cyclotron Laboratory Report No. 524, 1986.

[81] T. Suzuki, R. Fujimoto, and T. Otsuka, Phys. Rev. C **67**, 044302 (2003).

[82] S. Cohen and D. Kurath, Nucl. Phys. **73**, 1 (1965).

[83] A. E. L. Dieperink and T. de Forest, Phys. Rev. C **10**, 543 (1974).

[84] M. Leuschner, J. R. Calarco, F. W. Hersman, E. Jans, G. J. Kramer, L. Lapikás, G. van der Steenhoven, P. K. A. de Witt Huberts, H. P. Blok, N. Kalantar-Nayestanaki, and J. Friedrich, Phys. Rev. C **49**, 955 (1994).

[85] F. Resmini, R. M. L. Lombard, M. Pignanelli, J. L. Escudie, and A. Tarrats, Phys. Lett. B **37**, 275 (1971).

[86] Z. Y. Sun, D. Yan, S. T. Wang, S. W. Tang, X. H. Zhang, Y. H. Yu, K. Yue, L. X. Liu, Y. Zhou, F. Fang, J. D. Chen, J. L. Chen, P. Ma, and C. G. Lu, Phys. Rev. C **90**, 037601 (2014).

[87] C. Barbieri and W. H. Dickhoff, Int. J. Mod. Phys. A **24**, 2060 (2009).

[88] K. Ogata, K. Yoshida, and K. Minomo, Phys. Rev. C **92**, 034616 (2015).

[89] K. Ogata, Probing single-particle structures via proton-induced knockout reactions, 2015, The 13th RIBF discussion meeting on "Single-particle states from one-nucleon removal reactions".

[90] G. F. Grinyer, D. Bazin, A. Gade, J. A. Tostevin, P. Adrich, M. D. Bowen, B. A. Brown, C. M. Campbell, J. M. Cook, T. Glasmacher, S. McDaniel, A. Obertelli, K. Siwek, J. R. Terry, D. Weisshaar, and R. B. Wiringa, Phys. Rev. C **86**, 024315 (2012).

[91] J. Enders, T. Baumann, B. A. Brown, N. H. Frank, P. G. Hansen, P. R. Heckman, B. M. Sherrill, A. Stolz, M. Thoennessen, J. A. Tostevin, E. J. Tryggestad, S. Typel, and M. S. Wallace, Phys. Rev. C **67**, 064301 (2003).

[92] J. R. Terry, D. Bazin, B. A. Brown, J. Enders, T. Glasmacher, P. G. Hansen, B. M. Sherrill, and J. A. Tostevin, Phys. Rev. C **69**, 054306 (2004).

[93] N. Kobayashi, T. Nakamura, J. A. Tostevin, Y. Kondo, N. Aoi, H. Baba, S. Deguchi, J. Gibelin, M. Ishihara, Y. Kawada, T. Kubo, T. Motobayashi, T. Ohnishi, N. A. Orr, H. Otsu, H. Sakurai, Y. Satou, E. C. Simpson, T. Sumikama, H. Takeda, M. Takechi, S. Takeuchi, K. N. Tanaka, N. Tanaka, Y. Togano, and K. Yoneda, Phys. Rev. C **86**, 054604 (2012).

[94] C. A. Diget, P. Adrich, D. Bazin, M. D. Bowen, B. A. Brown, C. M. Campbell, J. M. Cook, A. Gade, T. Glasmacher, K. Hosier, S. McDaniel, D. McGlinchery, A. Obertelli, L. A. Riley, K. Siwek, J. R. Terry, J. A. Tostevin, and D. Weisshaar, Phys. Rev. C **77**, 064309 (2008).

[95] K. Wimmer, D. Bazin, A. Gade, J. A. Tostevin, T. Baugher, Z. Chajecki, D. Coupland, M. A. Famiano, T. K. Ghosh, G. F. Grinyer, M. E. Howard, M. Kilburn, W. G. Lynch, B. Manning, K. Meierbachtol, P. Quarterman, A. Ratkiewicz, A. Sanetullaev, R. H. Showalter, S. R. Stroberg, M. B. Tsang, D. Weisshaar, J. Winkelbauer, R. Winkler, and M. Youngs, Phys. Rev. C **90**, 064615 (2014).

[96] J. Enders, A. Bauer, D. Bazin, A. Bonaccorso, B. A. Brown, T. Glasmacher, P. G. Hansen, V. Maddalena, K. L. Miller, A. Navin, B. M. Sherrill, and J. A. Tostevin, Phys. Rev. C **65**, 034318 (2002).

[97] S. R. Stroberg, A. Gade, J. A. Tostevin, V. M. Bader, T. Baugher, D. Bazin, J. S. Berryman, B. A. Brown, C. M. Campbell, K. W. Kemper, C. Langer, E. Lunderberg, A. Lemasson, S. Noji, F. Recchia, C. Walz, D. Weisshaar, and S. J. Williams, Phys. Rev. C **90**, 034301 (2014).

[98] A. Gade, D. Bazin, B. A. Brown, C. M. Campbell, J. A. Church, D. C. Dinca, J. Enders, T. Glasmacher, P. G. Hansen, Z. Hu, K. W. Kemper, W. F. Mueller, H. Olliver, B. C. Perry, L. A. Riley, B. T. Roeder, B. M. Sherrill, J. R. Terry, J. A. Tostevin, and K. L. Yurkewicz, Phys. Rev. C **69**, 034311 (2004).

[99] A. Gade, D. Bazin, B. A. Brown, C. M. Campbell, J. A. Church, D. C. Dinca, J. Enders, T. Glasmacher, P. G. Hansen, Z. Hu, K. W. Kemper, W. F. Mueller, H. Olliver, B. C. Perry, L. A. Riley, B. T. Roeder, B. M. Sherrill, J. R. Terry, J. A. Tostevin, and K. L. Yurkewicz, Phys. Rev. Lett. **93**, 042501 (2004).

[100] A. Gade, D. Bazin, C. A. Bertulani, B. A. Brown, C. M. Campbell, J. A. Church, D. C. Dinca, J. Enders, T. Glasmacher, P. G. Hansen, Z. Hu, K. W. Kemper, W. F. Mueller, H. Olliver, B. C. Perry, L. A. Riley, B. T. Roeder, B. M. Sherrill, J. R. Terry, J. A. Tostevin, and K. L. Yurkewicz, Phys. Rev. C **71**, 051301 (2005).

[101] R. Shane, R. J. Charity, L. G. Sobotka, D. Bazin, B. A. Brown, A. Gade, G. F. Grinyer, S. McDaniel, A. Ratkiewicz, D. Weisshaar, A. Bonaccorso, and J. A. Tostevin, Phys. Rev. C **85**, 064612 (2012).

[102] K. L. Yurkewicz, D. Bazin, B. A. Brown, J. Enders, A. Gade, T. Glasmacher, P. G. Hansen, V. Maddalena, A. Navin, B. M. Sherrill, and J. A. Tostevin, Phys. Rev. C **74**, 024304 (2006).

[103] M. Yahiro, K. Ogata, and K. Minomo, Prog. Theor. Phys. **126**, 167 (2011).

[104] T. Aumann, C. A. Bertulani, and J. Ryckebusch, Phys. Rev. C **88**, 064610 (2013).

[105] M. Yasue, M. Tanaka, T. Hasegawa, K. Nisimura, H. Ohnuma, H. Shimizu, K. Ieki, H. Toyokawa, M. Iwase, J. Iimura, H. Yoshida, T. Nakagawa, A. Sato, T. Niizeki, J. Takamatsu, Y. Takahashi, T. Tohei, H. Orihara, T. Suehiro, S. Hayakawa, K. Ogawa, M. Igarashi, and R. Peterson, Nucl. Phys. A **509**, 141 (1990).

[106] G. Mairle and G. J. Wagner, Zeitschrift für Physik A Hadrons and Nuclei **258**, 321 (1973).

[107] G. Mairle, K. T. Knöpfle, P. Doll, H. Breuer, and G. J. Wagner, Nucl. Phys. A **280**, 97 (1977).

[108] T. Otsuka, R. Fujimoto, Y. Utsuno, B. A. Brown, M. Honma, and T. Mizusaki, Phys. Rev. Lett. **87**, 082502 (2001).

[109] T. Otsuka, T. Suzuki, R. Fujimoto, H. Grawe, and Y. Akaishi, Phys. Rev. Lett. **95**, 232502 (2005).

[110] K. Ogata, private communication.

[111] P. Kitching, C. A. Miller, W. C. Olsen, D. A. Hutcheon, W. J. McDonald, and A. W. Stetz, Nucl. Phys. A **340**, 423 (1980).